Glaciological and Chemical Studies on ice Cores from Hans Tausen Iskappe, Greenland

By Henrik B. Clausen, Mia Stampe, Claus Uffe Hammer, Christine S. Hvidberg, Dorthe Dahl-Jensen and Jørgen Peder Steffensen

Abstract

Clausen, H. B., M. Stampe, C. U. Hammer, C. S. Hvidberg, D. Dahl-Jensen and J. P. Steffensen 2001. Glaciological and Chemical Studies on ice Cores from Hans Tausen Iskappe, Greenland. Copenhagen, Danish Polar Center. Meddelelser om Grønland Geoscience 39, pp. 123-149.

The paper presents studies of various chemical and isotopical parameters from ice cores drilled in the northernmost located ice cap, Hans Tausen Iskappe, Pearyland, Greenland (HT). The 346 m main ice core (MC95) was drilled to bedrock in 1995 as well as a 35 m shallow core (SC95). A 60 m shallow core (SC75) and a 51 m shallow core (SC76) was drilled at two different positions in 1975 and 1976, respectively. A 6 m shallow core (SC94) was drilled in 1994. Continuous stable isotope records exist for all of these cores, total β-activity only from SC75 and SC76. Continuous ECM inferred acidity records exist along the 1995 cores (MC95 and SC95) and finally detailed records of dust and water soluble ion concentrations exist on selected parts of MC95.

To determine a time scale for the ice core is an important prerequisite for the interpretation of other records. The age scale is based on acid layers, caused by known volcanic eruptions, and by comparison of the chemical composition of these layers to that found in ice cores from other arctic locations. The total β-activity data from SC75 and SC76 provide fixed points to the time scale because a pronounced increase in total β-activity is related to the thermo-nuclear tests in the atmosphere in the early 1960'ies. Many of the investigated parameters exhibit seasonal variations e.g. $\delta^{18}O$, acidity, Cl^- and dust, therefore the study of the accumulation history of the ice cap improves our knowledge of the question if the mass balance of the Hans Tausen Iskappe is in equilibrium or not.

In the upper half part of the ice core the MC95 ECM record reveals several events of high acidity which can be connected to volcanic events known from other Greenland ice core records. Among the identified volcanic events are AD 1912 (Katmai, Alaska), AD 1815 (Tambora, Indonesia), AD 1783 (Laki, Iceland), AD 934 (Eldgjà, Iceland) and e.g. the signals of AD 1259 and 49 BC. The two latter signals originate from major volcanic eruptions of unknown eruption sites with a probable location close to the Equator in the case of the AD 1259 event. Some of the volcanic events are selected for an analysis of dust and water soluble chemical components, including F^-, $CH_3SO_2^-$, Cl^-, NO_3^-, SO_4^{2-}, Na^+, NH_4^+, K^+, Mg^{2+} and Ca^{2+}. Coulter counter technique was used for the dust measurements and the chemical analysis were carried out by ion chromatography.

Keywords: Ice cores; volcanism; ion chemistry; radioactivity; dating; precipitation.

H.B. Clausen, M. Stampe, C. U. Hammer, C. S. Hvidberg, D. Dahl-Jensen and J. P. Steffensen, University of Copenhagen, Department of Geophysics, Juliane Maries Vej 30, DK 2100 Copenhagen Ø, Denmark

Introduction

The Hans Tausen Iskappe (83°N, 38°W) in Pearyland, NE Greenland is one of the northernmost located glaciers in the world. This unique location close to the Greenland Sea and the Arctic Ocean combined with the fact that little information exists on past climate from this region, makes the Hans Tausen Iskappe a well suited place for performing palaeo-climatic and palaeo-environmental investigations by analysis of ice cores. For this reason ice cores have been drilled through 4 seasons: 1975-76 and 1994-95. The drilling sites are shown on Fig. 1, and the actual positions of the drilling sites, the length of the individual ice cores and their identifications (MC95, SC75 etc.) are given in Table 1.

In this work we want to concentrate on comparing the different records of ECM, water soluble ion chemistry, $\delta^{18}O$ and total β-acitivity in order to establish a reliable time scale and further to study the temporal and spatial distribution of the various components, e.g. the rate of annual accumulation and the acid deposition related to major volcanism.

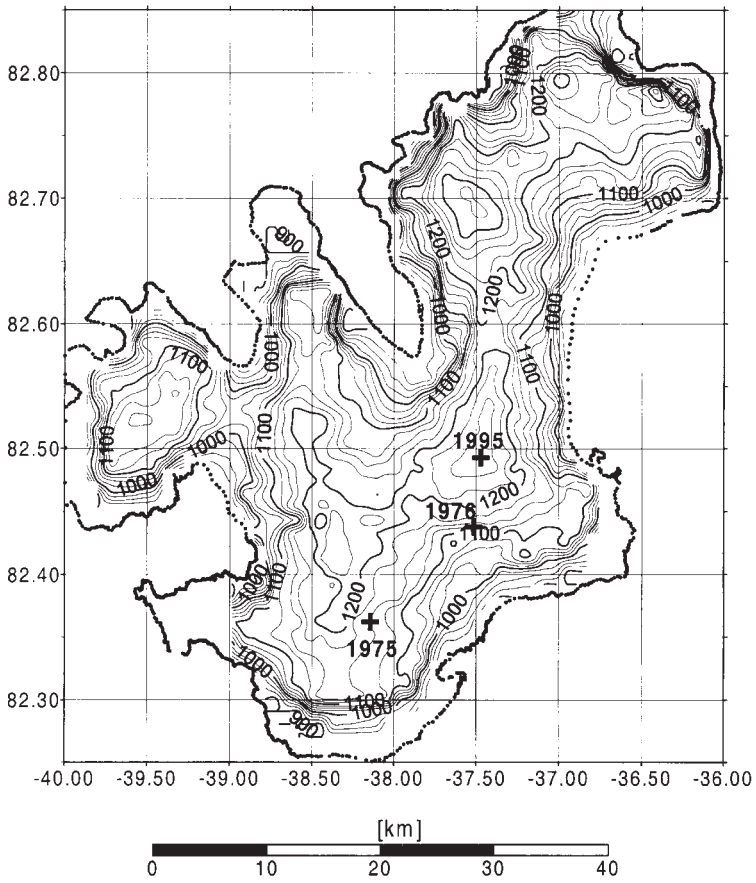

Fig. 1. The map shows the altitudes of the Hans Tausen Iskappe with 25 m contour lines and the positions of the 1975, 1976 and 1995 drilling sites presented in Table 1.

The ECM record

The ECM method reveals the acidity of polar ice by the measured electrical current on solid ice. The H^+ concentration is calculated based on an empirical relation between the electrical current and the H^+ concentration (Hammer 1980), (Clausen *et al.* 1995). The ECM record reveals several high acidity peaks which often are related to major volcanic eruptions in the northern hemisphere (see next section, The volcanic record).

In spite of the fact that Hans Tausen Iskappe is located at a high northern latitude (83°N) with an annual mean temperature of –21°C at a relative high altitude, 1275 m a.s.l., the summer air temperature often reaches 0°C or warmer, and rain occurs. These conditions imply that melting often takes place, and the water phase combined with a presence of alkaline dust, mainly from nearby local sources, has a great impact on the acid concentration of the snow pack, and causes neutralisation of the strong acids.

Year of drilling	Position °N	°W	Altitude m.a.s.l.	Type of core		Length of core, m	Rate of accumulation, m of ice equiv./year		Mean $\delta^{18}0$ per mil	Figs.
							0.162	1970-1975	–27,02	Figs. (22,23)
							0.152	1963-1975	–27,19	Figs. (22,24)
1975	82.38	38.28	1150	Shallow	SC75	60	0.152	1953-1975	–27,24	Figs. (22,24,26)
							0.155	1912-1975	–27,60	Fig. (26)
							0.147	1783-1975	–28,11	Fig. (26)
1976	82.43	37.50	1125	Shallow	SC76	51	0.147	1912-1976	–27,96	Figs. (24,26)
							0.141	1783-1976	–26,05	Figs. (24,26)
1994	82.51	37.47	1275	Handaugered	SC94	6	0.094	1975-1994	–26,27	Fig. (25)
							0.118	1970-1975	–26,05	Fig. (25)
							0.095	1975-1995	–26,31	Fig. (25)
							0.111	1970-1975	–25,53	Fig. (25)
				Main core	MC95	360	0.104	1963-1975	–25,84	Fig. (3)
1995	82.51	37.47	1275	and			0.113	1953-1975	–26,17	Figs. (3,24,26)
				shallow	SC95	35	0.114	1912-1995	–26,56	Figs. (3,24,26)
							0.108	1783-1995	–26,84	Figs. (3,26)

Table 1. Tabulates the positions of the different drilling sites shown on Fig. 1, as well as some compiled data of accumulation and $\delta^{18}O$ mean values for common periods represented in the different ice cores with references to the relevant figures.

The concentration of the strong acids in the snow precipitation is generally ~1-2 µequivalent H^+/kg snow, and the acids are mainly nitric acid and sulphuric acid.

The effect of the high summer air temperature is clearly seen in the melt layer percentage of the ice core. This parameter is some 5% at the surface layers, increasing to 15% at 150 m, to 70% at 250 m and reaches 100% at 275 m (Madsen and Thorsteinsson 2001). The ECM signal is seriously affected by the amount of melting. The frequency of high ECM signals decreases with the increased amount of the alkaline melt layers, thus at the depths below 250 m no distinct ECM signals appear (Fig. 2).

Another effect which makes it difficult to interpret the ECM signal is caused by the high air temperatures during part of the field season when the main core (MC95) was processed and the ECM measurements were performed. We use a reference temperature for ECM measurements at –14°C. MC95 was often measured at temperatures higher than –5°C. At these temperatures surface conductance may also occur through a water film, and the temperature correction factor which corrects the measured currents does not apply at these temperatures. The level of the ECM-signal exceeds by far the level of a signal measured at –14°C. However, the record can still be used to identify possible past major volcanism, but at 6 depth intervals hiatuses exist due to this temperature problem (Fig. 2 and Table 2). The shallow core SC95 was drilled, processed and ECM measured at the end of the field season at temperatures around –10°C, and this record shows "normal ECM behaviour" i.e. allows measured currents to be converted into H^+ concentrations by a conversion equation.

The comparison of the two ECM records from MC95 and SC95 over the last 230 years common in both records, is shown in Fig. 3 and Table 3. Normally we show the ECM records from ice cores in H^+ concentrations based on the actual measured currents, i, (in µAmp) corrected to –14°C and converted into concentrations (µequiv. H^+/kg of ice) by the original conversion equation:

$H^+ = 0.045 \cdot i^{1.73}$ (Hammer 1980). Due to the high temperature during the ECM

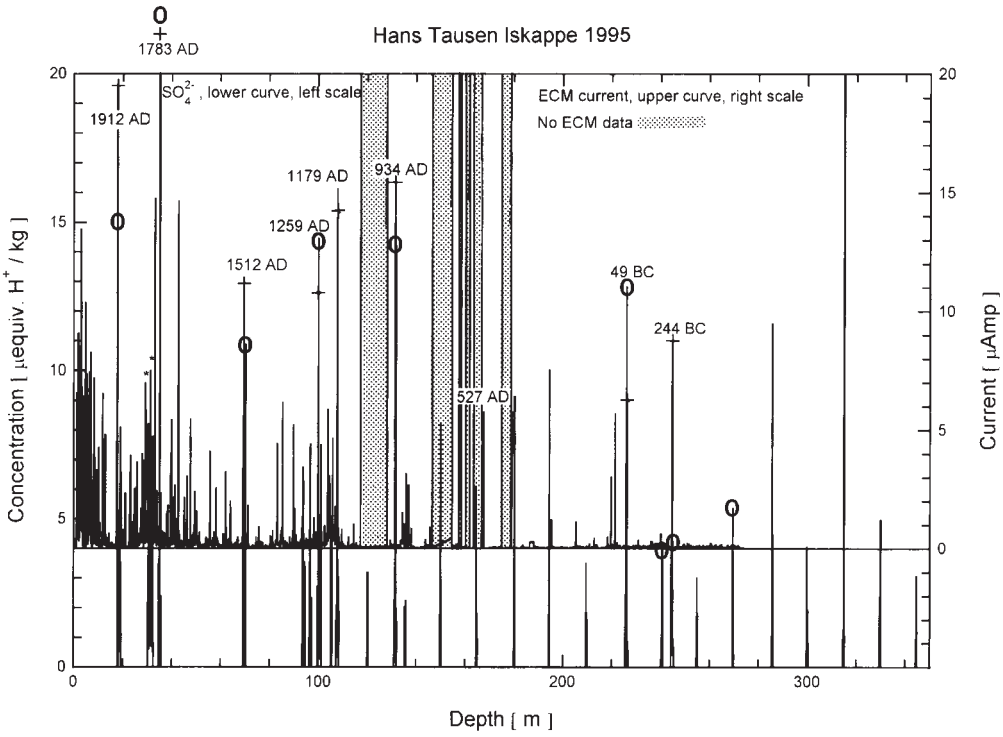

Fig. 2. The upper curve shows (on a depth scale) a continuous record of the actual measured ECM current (in µAmp, scale to the right). The data represent a resolution of 1cm. No ECM data exist for the dotted area, and the corresponding depth intervals are listed in Table 2. The lower curve shows (on the same depth scale) the actual measured sulphate concentration of selected depth intervals in 5 cm resolution. Some major volcanic signals are shown by their year of appearance in the ice core record. In the cases of overlap between current and concentration signals (above 250 m), two symbols are used to separate the signals:
o *means the maximum of the sulphate concentration value*
\+ *means the maximum of the current value.*
The peak values of the AD 1783 event are 39 units and 33 units for sulphate and current, respectively.

The two asterisks around 30 and 31 m correspond to the volcanic signals of AD 1816 and AD 1810. A detailed version of the current for the top 40 m is shown in Fig. 3, and detailed sulphate values for 4 depth intervals around the AD 1512, AD 1179, 49 BC and 244 BC events are shown on Figs. (15, 17, 19, 21), respectively.

measurements and the high content of alkaline material in the ice, we use the actual measured currents corrected to –14°C in the case of SC95, and in the case of MC95 we use the actual measured currents because the currents are generally measured at temperatures above –5°C. Fig. 4 exhibits the effect of the high temperature on the actual measured electrical currents. 5 prominent volcanic events (exhibited in Fig. 3 as #4, 5, 10, 11 and 12) from the last 200 years are used in the comparison which shows that at temperatures above –5°C a substantial and uncontrollable surface conductance takes place through a water film, and this effect is not accounted for by the ordinary calibration curve.

The actual measured temperatures are

Table 2. Exhibits the depth intervals of the missing ECM data from MC95, and the corresponding ages of the ECM hiatuses which are presented as dotted areas on Figs. 2 and 6.

Depth Interval m	Time Interval Age, year AD
117.15-128.15	1080-965
146.30-154.55	766-673
156.75-158.40	649-630
160.05-161.70	613-594
163.35-166.65	575-538
174.90-178.75	456-418

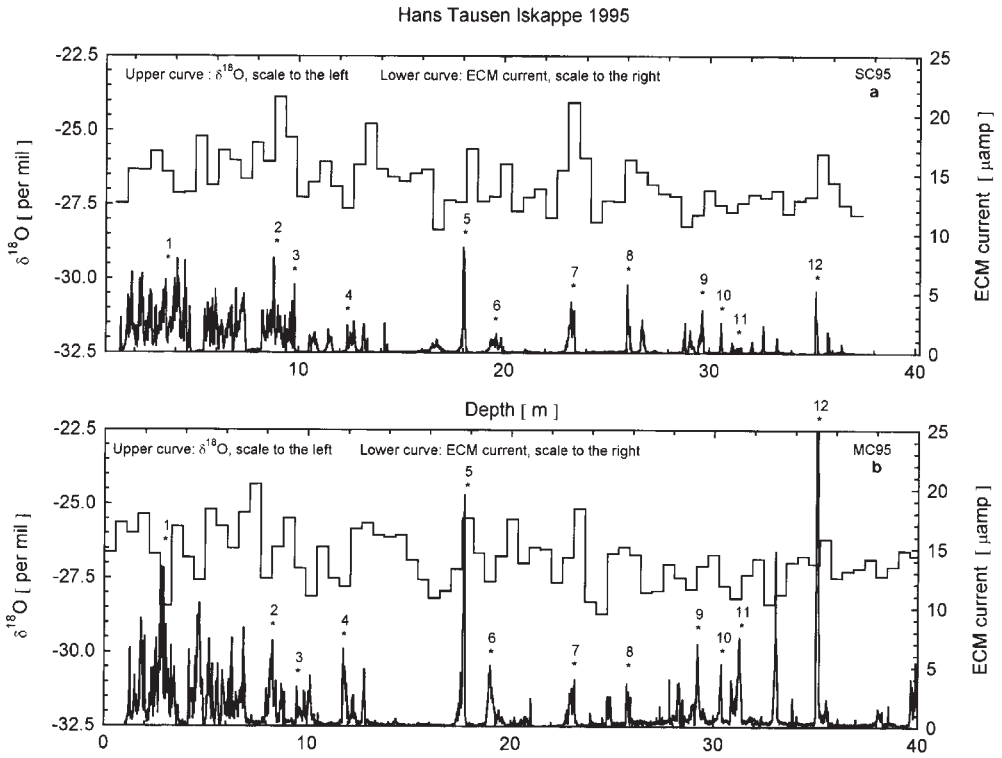

Fig. 3. The $\delta^{18}O$ records in 55 cm resolution from HT95SC and HT95MC are shown at the top of figs. a and b, respectively. The bottom curve of fig. a shows the actual measured ECM-currents referenced to –14°C, in the case of fig. b the actual measured ECM currents are shown. The numbered asterisks (#1-#12) correspond to common events in the two records: #5 and #12 : the Katmai 1912 and the Laki 1783 eruptions. These major volcanic events are used to lock the two records together. For both records the actual surface at the time of drilling serves as the depth reference, thus the difference in the depth for the same event in the two records is due to the different drilling time of MC95 and SC95. The MC95 core is drilled at the start of the season, and SC95 some 6 weeks later when new snow falls had added some 60 cm of snow at the surface.

According to (Simkin and Siebert 1994) 13 out of the 16 largest explosive volcanic eruptions of the 19th and the 20th century took place north of 20°S. Of these 13 events 7 were located between 20°S and 20°N: 1991, Pinatubo, Philippines; 1982, El Chichon, Mexico, (1); 1902, Santa Maria, Guatemala, (6); 1883, Krakatau, Indonesia; 1835, Cosiguina, Nicaragua; 1822, Galunggung, Indonesia, (9) and 1815, Tambora, Indonesia, (10), one event between 20°N and 50°N:1980, Mt. St. Helens, USA and 5 events at higher latitudes than 50°N: 1956, Bezymianny, Kamchatka, (3); 1912, Katmai, Alaska, (5); 1907, Ksudach, Kamchatka; 1875, Askja, Iceland, (7) and 1854, Sheveluch, Kamchatka, (8).

The numbers in parentheses correspond to the asterisk # of the figure.

Besides these events, #2, 4 and 11 are assigned to 1963, Agung, Indonesia; 1947, Hekla, Iceland and 1810, unknown, respectively.

shown in Fig. 5 where the numbers 1 through 12 correspond to those of Fig. 3.

The volcanic record

Major volcanic eruptions emit large amounts of acid gasses into the atmosphere, mainly SO_2 which eventually ends up as H_2SO_4. The acid is deposited at the snow surface by precipitation and can in an ice core be identified by the ECM method as layers with increased H^+ concentration. A continuous record of major volcanism of the last 4000 years, obtained by an ice core from the GRIP site in central Greenland, reveal some 50

Table 3. Displays the average ice thickness of the annual layers (λ) between the fixed points for the common periods in MC95 and SC95 based on acid volcanic layers determined by ECM.

		MC95 λ			SC95 λ	
Age year AD/BC +/–	**Depth at signal**	**from fixed point to 1995**	**between fixed points**	**Depth at signal**	**from fixed point to 1995**	**between fixed points**
		m of ice/year			**m of ice/year**	
1995	0			0		
1983	1.06	0.008	0.088	1.34	0.112	0.112
1963	3.68	0.115	0.131	3.95	0.123	0.131
1947	5.66	0.118	0.124	6.02	0.125	0.130
1912	9.49	0.114	0.109	9.68	0.117	0.104
1816	19.08	0.107	0.100	19.24	0.108	0.100
1810	19.81	0.107	0.122	20.03	0.108	0.131
1783	22.99	0.108	0.118	23.09	0.109	0.113
1512	54.65	0.113	0.117			
1259	84.50	0.115	0.118			
1179	92.12	0.113	0.095			
934	115.74	0.109	0.096			
527	152.03	0.104	0.089			
-49	210.55	0.103	0.102			
-244	229.06	0.102	0.095			

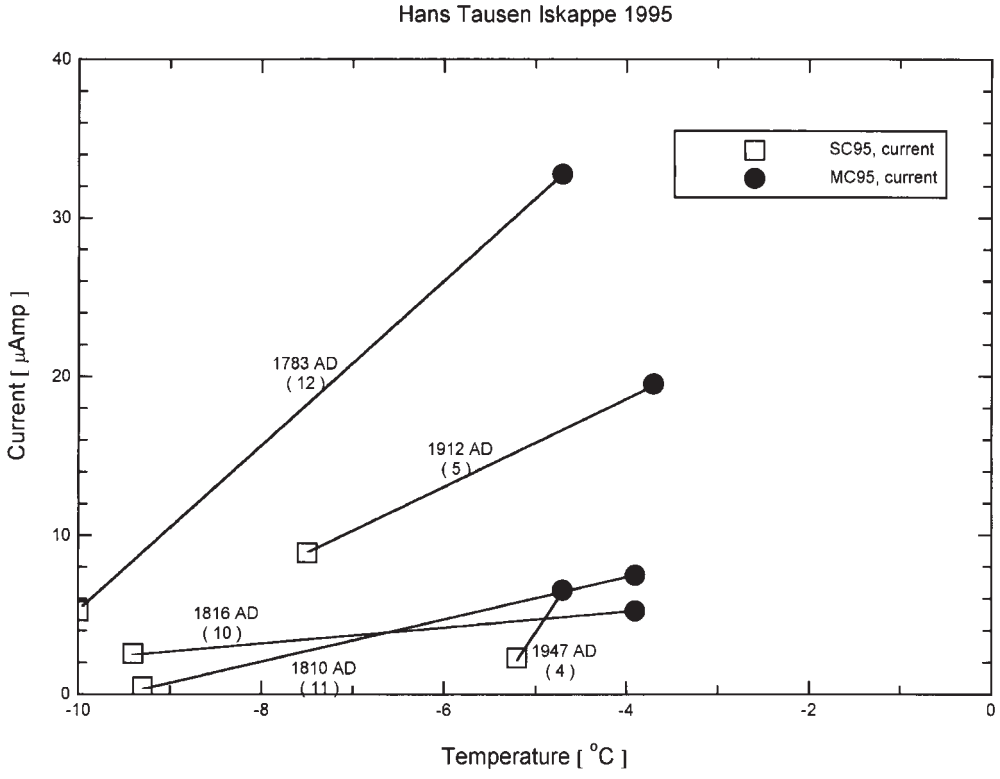

Fig. 4. The peak values of the ECM currents for 5 different volcanic events, identified in HT95SC and HT95MC, are plotted versus the temperature of the ECM measurements. The currents are corrected to –14°C for the HT95SC values. The graph clearly exhibits the uncontrollable effect of the high temperature on the ECM currents. The numbers in parentheses correspond to the numbers of Fig. 3.

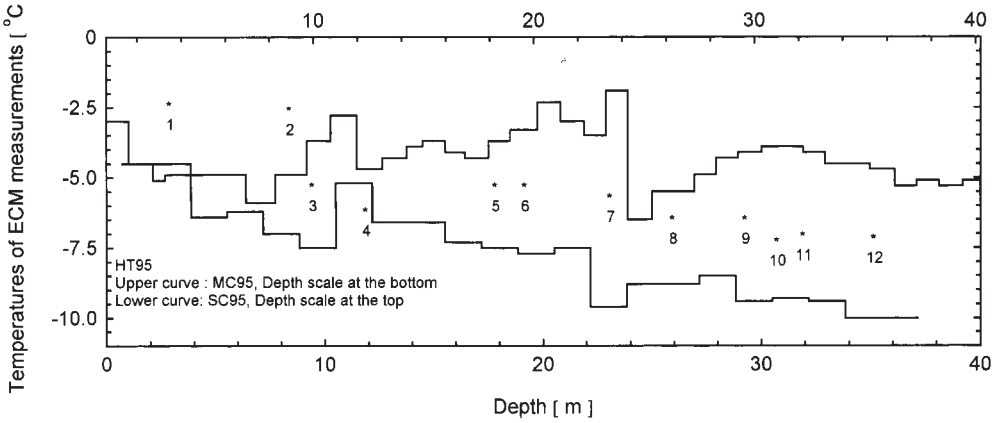

Fig. 5. The actual temperatures of the ECM measurements. The numbered asterisks correspond to the numbers shown in Fig. 3.

major volcanic events from the last 2000 years (Clausen *et al.* 1997) which are relevant for the comparison in this paper. Of these 50 events, 13 belong to the category of the strongest signals characterized by a strong acid deposition rate on the ice surface of more than 3 times the natural acid background deposition rate, and a duration of increased acidity over a time interval of one year or more. Fig. 3 exhibits among others 4 of these 50 volcanic events: AD 1912, 1816, 1810 and 1783, found in the time interval common of HT95MC and HT95SC. Fig. 6 shows at the top: the peak current values of the continuous HT95MC ECM record (shown as upper curve in Fig. 2) on a time scale, and at the bottom: the sulphuric acid deposition at GRIP on the same time scale. Of the 13 major events mentioned above: AD 1783, 1512, 1259, 1229, 1179, 934, 871, 645, 527, 514, 159, 49 BC and 244 BC, the 8 underlined events are used as fixed points for the time scale.

Ages of the acid signals located

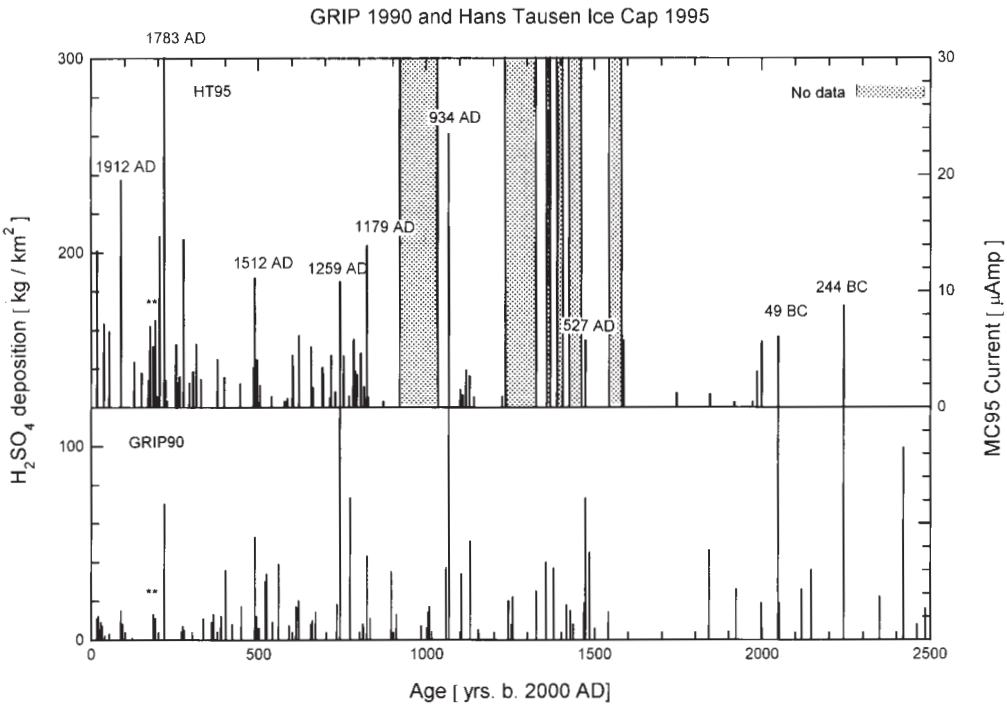

Fig. 6. The upper curve shows (on a time scale) the maximum value of the observed electrical currents of the ECM measurements (scale to the right). Table 4 lists these currents as well as the ice temperature during the ECM measurements. The dotted area correspond to the depths intervals listed in Table 2. The lower curve shows (on the same time scale) the volcanic H_2SO_4 deposition at the GRIP site in central Greenland (scale to the left). The basis of the time scale is the major volcanic eruptions given by their year of appearance in the GRIP ice core record (Clausen et al. 1997).

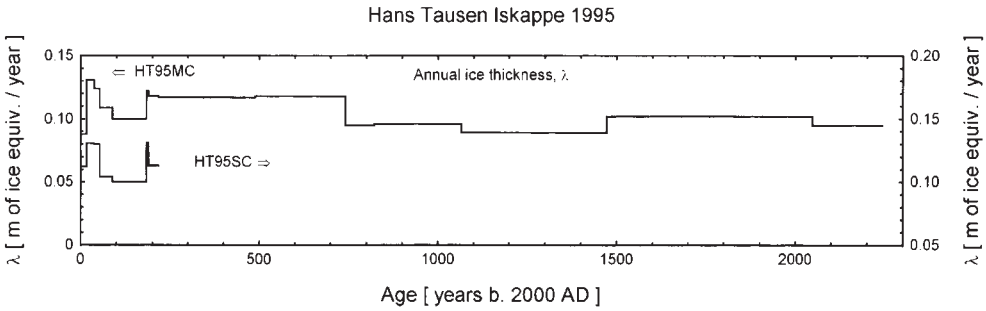

Fig. 7 exhibits the annual ice thicknesses, λ, for the 95MC and the 95SC ice cores based on the fixed points given in Tables 3 and 4.

between the fixed points are found by linear interpolation based on the rate of the annual ice thickness determined by the depths of the fixed points. An interesting observation is that no significant thinning of annual layers versus depth is observed. This indicates that Hans Tausen Iskappe is not in mass balance, and analysis of surface movements in relation to the accumulation rate by Keller *et al.* (2001) shows that the ice cap is not in mass balance at present. The annual ice thicknesses are displayed in Table 3 and shown in Fig. 7 for the common periods of HT95MC and HT95SC.

Table 4 shows it in details for the period AD 1995 to 244 BC, and we see that of the 5 major volcanic events: AD 1229, 871, 645, 514, and 159, not accounted for above, the 3 underlined show up as AD 1232, 871, and 156, respectively. Besides these events we also see other prominent volcanic signals known from GRIP, like AD 1601, 1554, 898 and 79, show up as AD 1605, 1557, 898 and 83, respectively. As to the discussion of the chemical composition of the volcanic signals, see next section.

The chemical record

Determination of the concentration of water soluble inorganic components have been performed on selected sections of the ice core and the intervals of sampling are shown on the lower curve in Fig. 2 by the sulphate concentrations together with the ECM currents on a common depth scale. The ionic concentration measurements are performed by ion chromatography and the insoluble particle (dust) concentrations done on the snow pit samples are determined by Coulter counter technique.

First we discuss the various components, their interaction, and compare the records to values measured on the GRIP ice core. This study is based on some 570 samples (each 5 cm) representing the depth intervals of the ice core shown on Figs. 2 and 8-12. A compilation of the data is presented in Table 5.

All chemical concentration data are given in the unit µequivalent per kg of ice (µequiv./kg) and the components discussed here are the anions and cations listed below with their natural sources given in decreasing order of importance:

Mg^{2+}	terrestrial, marine
Ca^{2+}	terrestrial, marine
Na^{+}	marine, terrestrial
Cl^{-}	marine, volcanic, terrestrial
F^{-}	volcanic
SO_4^{2-}	volcanic, biological (terrestrial and marine), terrestrial
NH_4^{+}	biological (terrestrial)
NO_3^{-}	atmospheric
K^{+}	terrestrial
$CH_3SO_3^{-}$ (MSA)	marine

For references to the sources see e.g. Clausen and Langway (1989), Legrand *et al.* (1997) and Wolff (1995).

Age year AD/BC +/–	Depth at signal m of snow	Depth at signal m of ice	λ from fixed point to 1995 m of ice/year	λ between fixed points	Current i µAmp	Measured temp. °C
1995*	0	0				
1983*	2.790	1.061	0.088	0.088	13.46	– 4.9
1963*	8.280	3.680	0.115	0.131	7.20	– 4.9
1947*	11.760	5.660	0.118	0.124	6.54	– 4.7
1912*	17.710	9.490	0.114	0.109	19.54	– 3.7
1873	23.150	13.411		0.100	3.88	– 1.9
1852	25.800	15.480		0.100	2.94	– 5.5
1831	28.490	17.550		0.100	2.30	– 4.3
1826	29.200	18.120		0.100	6.99	– 4.1
1816*	30.370	19.075	0.107	0.100	5.24	– 3.9
1813	30.850	19.475		0.122	3.93	– 3.9
1810*	31.250	19.805	0.107	0.122	7.50	– 3.9
1806	31.890	20.328		0.118	0.82	– 3.9
1802	32.370	20.726		0.118	0.92	– 4.1
1797	33.040	21.284		0.118	14.74	– 4.5
1783*	35.070	22.994	0.108	0.118	32.75	– 4.7
1780	35.520	23.376		0.117	2.30	– 4.7
1749	39.650	26.940		0.117	4.02	– 5.1
1748	39.880	27.145		0.117	5.43	– 5.1
1743	40.490	27.681		0.117	2.08	– 5.1
1737	41.300	28.395		0.117	2.63	– 4.5
1726	42.700	29.628		0.117	14.45	– 4.5
1708	45.140	31.822		0.117	2.08	– 4.5
1698	46.370	32.933		0.117	3.05	– 4.9
1688	47.700	34.141		0.117	5.47	– 4.9
1674	49.520	35.805		0.117	2.37	– 3.5
1625	55.600	41.452		0.117	4.11	– 3.9
1605	58.120	43.809		0.117	2.57	– 3.0
1557	64.030	49.418		0.117	2.01	– 2.3
1516	69.090	54.273		0.117	3.38	– 2.8
1512*	69.480	54.648	0.113	0.117	11.16	– 2.8
1509	69.920	55.073		0.118	3.16	– 2.8
1506	70.240	55.381		0.118	4.07	– 2.8
1497	71.300	56.406		0.118	1.85	– 2.6
1462	75.580	60.556		0.118	0.92	– 2.6
1399	83.100	67.898		0.118	4.43	– 3.7
1399	83.180	67.976		0.118	2.44	– 3.7
1398	83.290	68.084		0.118	3.48	– 3.7
1380	85.390	70.143		0.118	6.18	– 3.7
1343	89.790	74.470		0.118	5.20	– 1.9
1338	90.380	75.051		0.118	1.68	– 1.9
1310	93.720	78.345		0.118	3.43	– 1.1
1308	93.930	78.552		0.118	2.88	– 1.1
1284	96.750	81.338		0.118	4.43	– 1.5

Table 4. Shows the ages of the acid layers of the MC95 record from AD 1995 back to 244 BC. The ages of the acid signals located between the fixed points (marked by asterisks) are found by interpolation based on the rate of the annual ice thickness (λ) determined by the depths of the fixed points. Also presented are the actual measured maximum electrical currents of the individual acid peaks (in the units µAmp), and the actual temperature of the ice during the ECM measurements.

Table 4. Cont.

Age year AD/BC +/–	Depth at signal m of snow	Depth at signal m of ice	λ from fixed point to 1995 m of ice/year	λ between fixed points m of ice/year	Current i μAmp	Measured temp. °C
1272	98.240	82.811		0.118	1.29	– 1.9
1259*	99.950	84.504	0.115	0.118	10.80	– 2.3
1248	101.050	85.593		0.095	4.38	– 2.3
1232	102.520	87.050		0.095	0.95	– 2.3
1219	103.820	88.348		0.095	2.44	– 1.9
1218	103.900	88.427		0.095	5.86	– 1.9
1213	104.330	88.854		0.095	3.05	– 1.9
1209	104.700	89.211		0.095	2.76	– 1.9
1197	105.850	90.351		0.095	4.64	– 1.6
1187	106.850	91.374		0.095	1.76	– 1.1
1179*	107.630	92.118	0.113	0.095	13.93	– 1.1
1130	112.350	96.807		0.096	0.49	– 6.6
934*	131.360	115.739	0.109	0.096	15.47	– 2.6
900	134.370	118.742		0.089	1.51	– 2.3
898	134.550	118.921		0.089	1.01	– 2.3
893	135.030	119.400		0.089	1.03	– 2.3
883	135.880	120.248		0.089	3.16	– 1.4
872	136.870	121.236		0.089	2.69	– 1.4
775	145.530	129.930		0.089	0.91	– 3.7
527*	167.630	152.030	0.104	0.089	5.76	– 4.7
417	178.810	163.210		0.102	1.24	– 12.4
414	179.110	163.510		0.102	5.76	– 12.4
255	195.360	179.760		0.102	1.20	– 8.5
156	205.380	189.780		0.102	1.12	– 9.0
83	212.840	197.240		0.102	0.42	– 5.0
29	218.290	202.690		0.102	0.47	– 4.8
16	219.610	204.010		0.102	3.05	– 4.7
1	221.210	205.610		0.102	5.69	– 4.3
– 49*	226.150	210.550	0.103	0.102	6.07	– 4.3
–244*	244.660	229.060	0.102	0.095	8.75	– 7.3

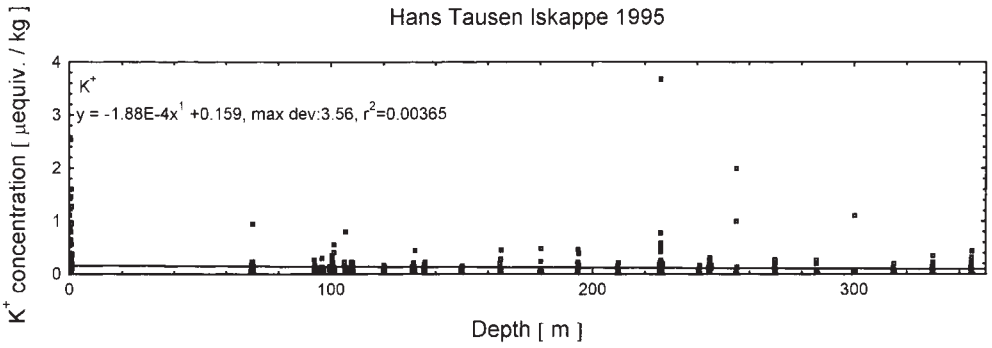

Fig. 8 shows a slightly decreasing concentration of the terrestrial component K^+ versus depth.

Compound	Mean values of concentration [µequiv. / kg]			Figs.
	Measured	Graphic		
Cl^-	1.29	0.88 – 1.84, 1.36	Increase vs. depth	Fig. 10
Na^+	0.96	0.64 – 1.24, 0.94	Increase vs. depth	Fig. 10
Na^+_{ss}	0.89			
Ca^{2+}	5.47	1.07 – 11.05, 6.06	Increase vs. depth	Fig. 9
Ca^{2+}_{nss}	5.43			
Mg^{2+}	2.37	0.44 – 4.54, 2.49	Increase vs. depth	Fig. 9
Mg^{2+}_{nss}	2.17			
SO_4^{2-}	2.08	1.82 – 2.18, 2.00	Increase vs. depth	Fig. 11
$SO_4^{2-}{}_{nss}$	1.97			
NO_3^-	1.18	1.36 – 0.94, 1.15	Decrease vs. depth	Fig. 12
K^+	0.14	0.16 – 0.09, 0.13	Decrease vs. depth	Fig. 8

Table 5. Compiles the mean value of various chemical compounds with references to the relevant figures.

The chemical data sets are corrected for their marine contributions:

$$Na^+_{ter} = 0.5K^+ \quad (1)$$

$$Na^+ = Na^+_{ss} + Na^+_{ter}\,;\, Na^+_{ss} = Na^+ - 0.5K^+ \quad (2)$$

$$Cl^-_{ex} = Cl^- - 1.166\, Na^+_{ss} \quad (3)$$

$$Mg^{2+}_{nss} = Mg^{2+} - 0.228Na^+_{ss} \quad (4)$$

$$Ca^{2+}_{nss} = Ca^{2+} - 0.0436Na^+_{ss} \quad (5)$$

$$SO_4^{2-}{}_{nss} = SO_4^{2-} - 0.120\, Na^+_{ss} \quad (6)$$

Here the chemical symbol (e.g. Na^+) means the actual measured concentra-

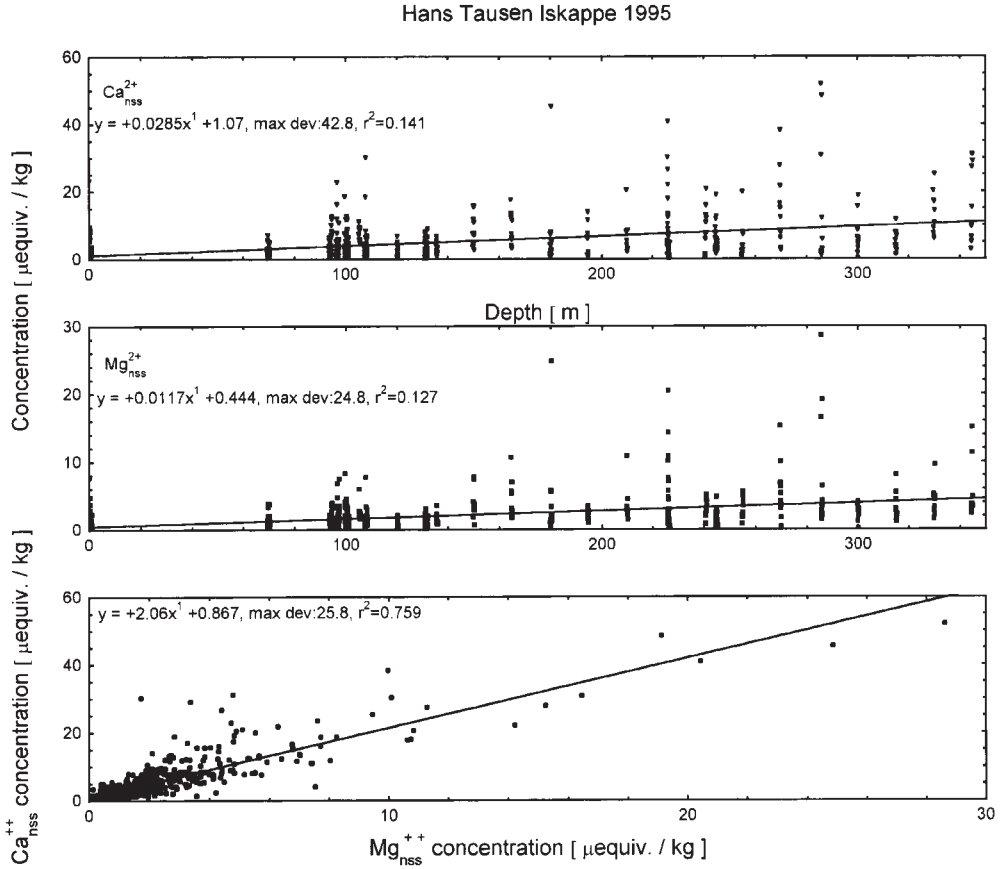

Fig. 9 shows an increasing concentration of non sea salt Ca^{2+} and Mg^{2+} versus depth, and Ca^{2+}_{nss} plotted versus Mg^{2+}_{nss} determines a concentration ratio around 2 for these dominating impurities, indicating a dolomite type of impurity source.

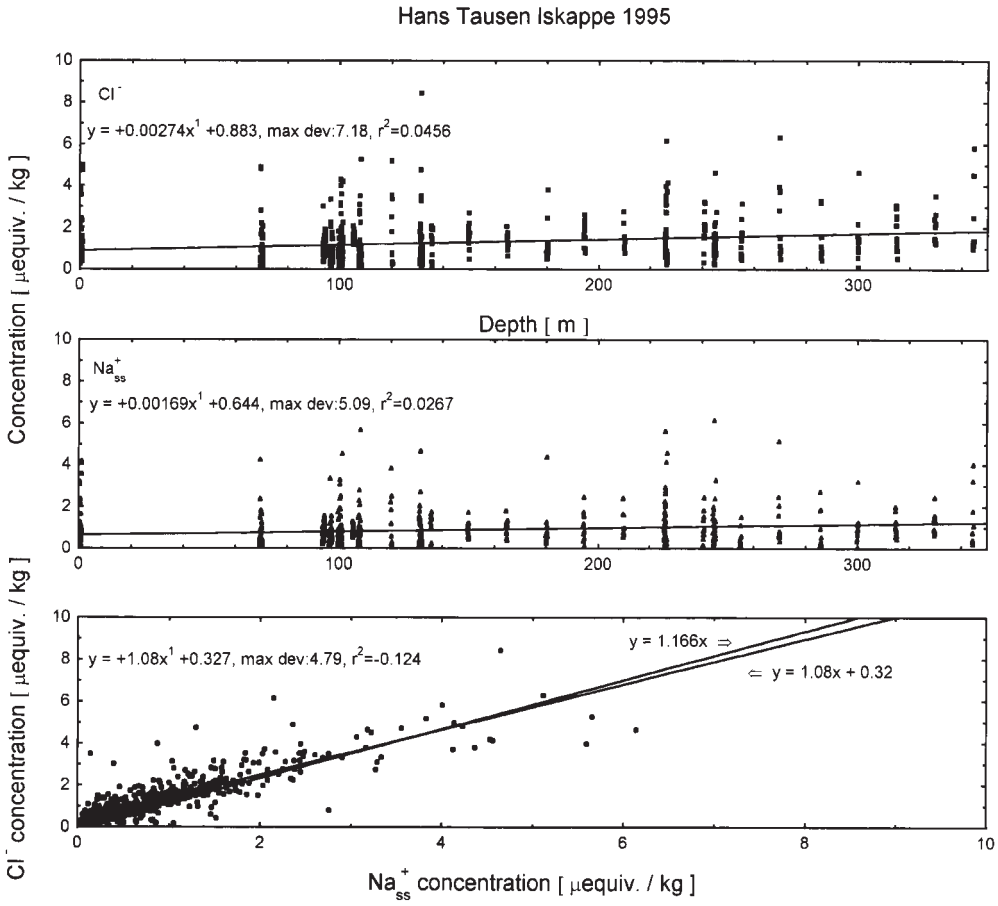

Fig. 10 shows an increasing concentration of Cl^- and sea salt Na^+ versus depth, and Cl^- plotted versus Na^+_{ss} determines a concentration ratio typical for sea salt.

tion, and the chemical symbols provided with the lowered symbols **ss**, **nss** , **ter**, and **ex** refer to the element concentration of sea salt, non sea salt, terrestrial matter and excess amount, respectively. The sea salt concentration ratios, based on the unit µequiv./kg, for the different components relative to Na^+_{ss} are 1.166, 0.120, 0.228 and 0.0436 for Cl^-_{ss}, SO^{2-}_{4ss}, Mg^{2+}_{ss} and Ca^{2+}_{ss}, respectively (Sverdrup *et al.* 1942). Thus Cl^-_{ex} means Cl^-_{nss}, e.g. present as HCl.

K^+ is of terrestrial origin, with an average concentration level of 0.15 µequiv./kg over the entire ice core varying from 0.16 to 0.10 µequiv./kg at the top and bottom, respectively (Fig. 8) with a maximum deviation of some 4 µequiv./kg. The concentration is higher than at GRIP where the typical concen-

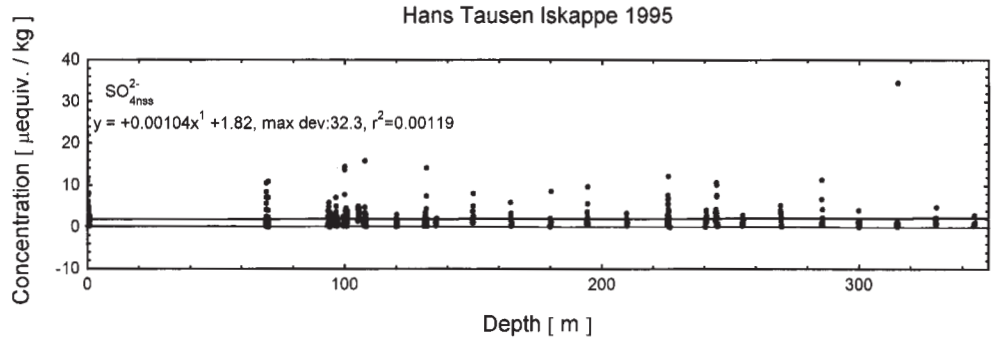

Fig. 11 shows a slightly increasing concentration of non sea salt sulfate versus depth.

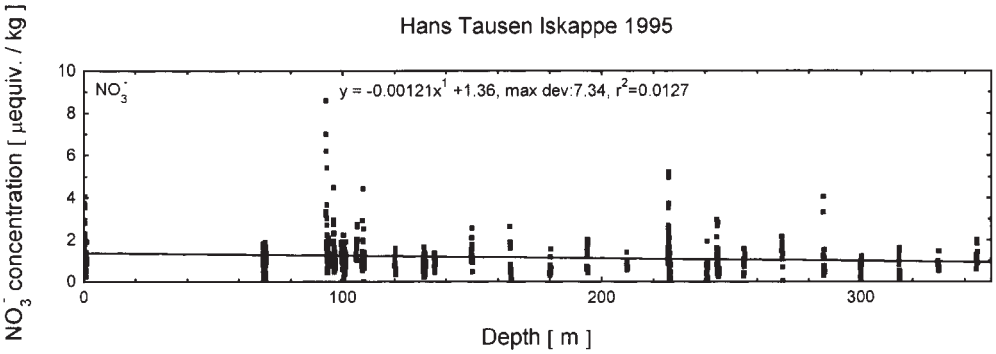

Fig. 12 shows a nearly constant concentration level of the atmospheric component NO_3^- versus depth, indicating that no essential source strength variations has occurred during the time period represented in the record.

tration levels are around 0.05 µequiv./kg.

Na^+ is mainly of marine origin, and for Holocene ice from central parts of Greenland the concentration of this component can be used to correct the concentration of other ions like SO_4^{2-}, Mg^{2+} etc. for their sea salt contribution. Hans Tausen Iskappe is located close to the ice free margin of the Greenland ice cap, therefore the concentrations of ions originating from local terrestrial sources exceed by far those found in ice from central parts of the ice cap (Steffensen *et al.* 2001). Ca^{2+} and Mg^{2+} are the main components of the impurities of the HT ice core (Fig. 9). The main source of these components are limestone and dolomite with some shales which are present in the HT glacier area of NE Greenland. (Blaker and Peel 1997). Because a considerable amount of K^+ is found, we use this component to correct the Na^+ content for its terrestrial contribution. According to Handbook of Geochemistry (Wedepohl 1969) we use a value of 0.5 for the Na^+/K^+ ratio of dolomite sediments to correct the Na^+ for the terrestrial component (1). The actual measured Cl^- / Na^+ ratio is in average 1.4, and for Na^+ corrected for Na^+_{ter} according to (2), we get 1.5 (Table 5) compared to a seawater ratio of 1.17 which is the typically value determined in ice from central parts of Greenland where deviations from this value in the form of excess Cl^- (Cl^-_{ex}) are especially observed in the acid ECM peaks related to Icelandic volcanism (Clausen *et al.* 1997). Fig. 10 suggests a Cl^-/Na^+ ratio of 1.08, which like the above mentioned values are not significant different from the sea water ratio considering the large deviations of the values displayed in Fig.10.

Fig. 9 and Table 5 show a Ca^{2+}_{nss} / Mg^{2+}_{nss} ratio of 2-2.5 and a concentration increase of the two elements versus depth. This ratio is a strong indicator that dolomite is the main contributor of the Ca^{2+} and Mg^{2+} impurities. The increasing rates of concentration with depth indicate that the altitude of the glacier surface has been increasing during the life time of the glacier (Keller *et al.* 2001; Hammer *et al.* 2001).

Fig. 11 and Table 5 show an average SO^{2-}_{4nss} concentration of 2-2.5 equiv./kg with slightly increasing values versus depth. A substantial amount of the sulphate content is conneceted to the terrestrial source.

Fig. 12 and Table 5 show an average NO_3^- concentration of 1.2 µequiv./kg with a constant level versus depth. The shown decrease versus depth can not be considered to be significant due to the high variability. The concentration level is similar to levels found at other Greenland locations, and the high variability is due to the frequent melting at the HT site (Clausen *et al.* 1995).

Secondly we discuss the concentration of various ions with special emphasis on

Table 6. Displays the annual ice thicknesses around 4 distinct volcanic events (AD 1179, AD 1512, 49 BC and 244 BC) based on the chemical components Ca^{2+} and Mg^{2+}, Na^{+} and Cl^{-}, NH_4^{+} and NO_3^{-} which all show seasonal variations (see Figs. 14-21). The values, based on only 5-10 years, are not inconsistent with the values (in parentheses) from Table 3.

Depth Interval of 2,5 cm samples m	Age of volcanic event Year AD / BC	Number of annual layers based on: Ca^{2+} / Mg^{2+}	Na^{+} / Cl^{-}	NH_4^{+} / NO_3^{-}	Average of annual ice thickness cm of ice eq./year
69.30- 70.40	AD 1512	10 ± 1	10 ± 1	10 ± 1	11 ± 1 (11.7)
107.25-108.35	AD 1179	10 ± 1	10 ± 1	10 ± 1	11 ± 1 (9.5)
225.80-226.35	49 BC	6 ± 1	6 ± 1	6 ± 1	9 ± 1 (10.2)
244.35-244.90	244 BC	5 ± 0.5	5 ± 0.5	5 ± 0.5	11 ± 1 (9.5)

the dating of the ice core. The data for this are detailed chemistry profiles (2.5 cm per sample) from a snow pit study covering the top one meter of snow (Fig. 13), and from 4 depth intervals around pronounced acid signals originating from the distinct volcanic eruptions of AD 1512, AD 1179, 49 BC and 244BC given in Table 6 and shown in Figs. 14-21. Fig. 13 show a detailed $\delta^{18}O$ profile from a surface snow pit. The profile clearly exhibits the seasonality of the years 1992 to 1994.The seasonality is also seen in the Na^{+} and Cl^{-} profiles with the characteristic peak in the winter precipitation (in the $\delta^{18}O$ minimum). A Cl^{-} to Na^{+} ratio of 1.14 is close to the sea salt ratio of 1.17 for the two elements. The seasonality is also observed in the Ca^{2+} and Mg^{2+} concentrations with a ratio around 2. In snow from central parts of Greenland the seasonality exhibited by the dust concentration (insoluble particles) varies in parallel with Ca^{2+} concentration with maximum in early spring precipitation (Hammer 1977). This be-

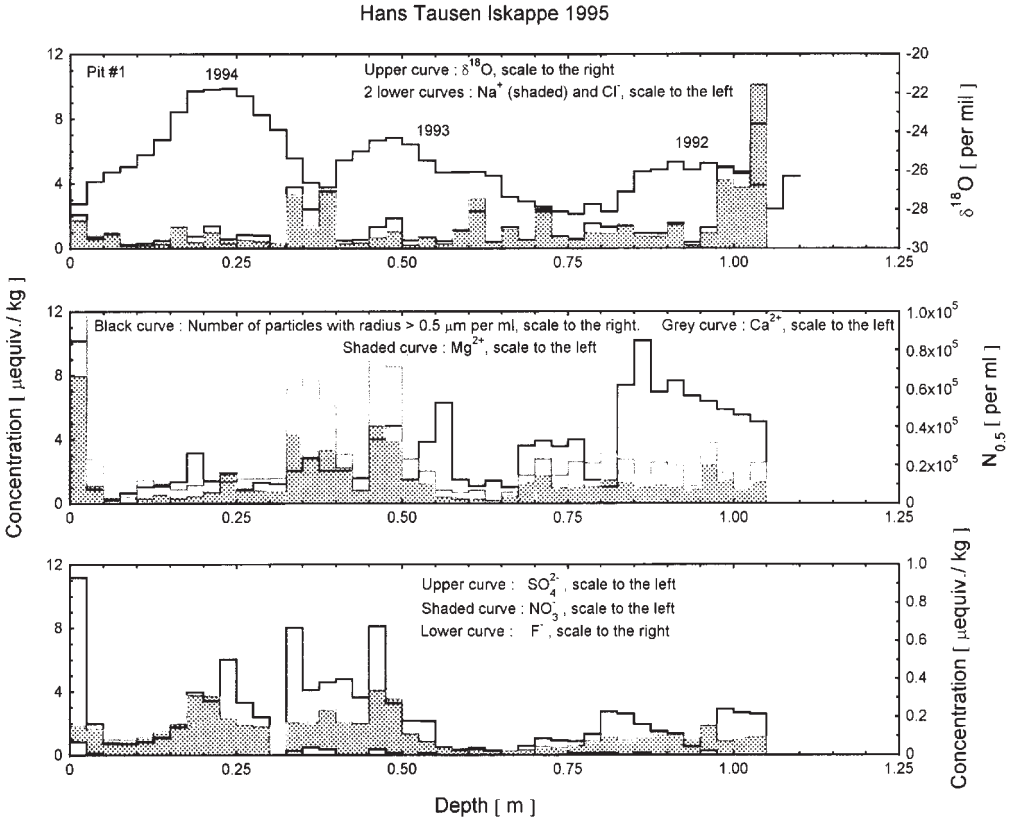

Fig. 13 presents detailed profiles of $\delta^{18}O$, insoluble particles and 7 water soluble chemical components (Na^{+} and Cl^{-}, Mg^{2+} and Ca^{2+}, NO_3^{-}, SO_4^{2-} and F^{-}). The $\delta^{18}O$ curve is shown with calendar years at the summer positions. The winter layers are indicated by the maxima of the Na^{+} and Cl^{-} concentration, and the spring layers by maximum of Mg^{2+} and Ca^{2+} concentration and of dust concentration. The summer layers are exhibited in the NO_3^{-} peaks (see the text for details).

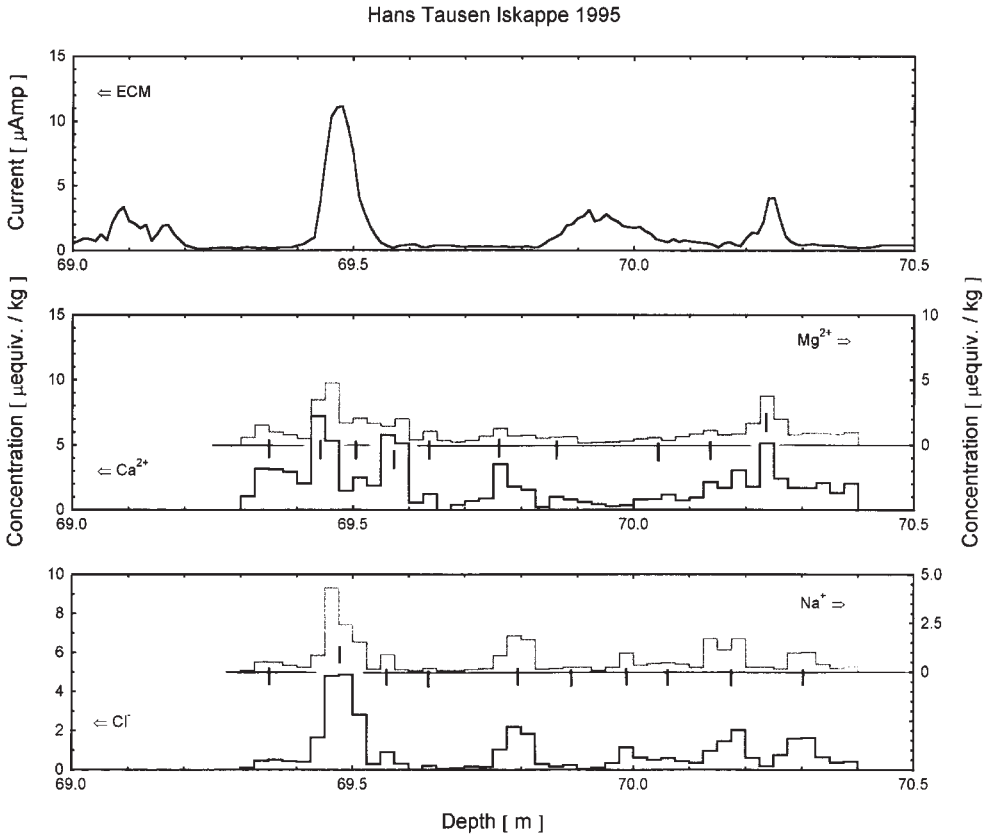

Fig. 14.

Figs. 14, 16, 18 and 20 show detailed profiles of ECM current, Mg^{2+}, Ca^{2+} and Na^{+}, Cl^{-} concentrations at 4 depth intervals around the distinct volcanic events of AD 1512, AD 1179, 49 BC and 244 BC. In the case of the AD 1179 event (Fig. 16) a detailed δ18O record is shown as well. The vertical marking on the records with a resolution of 2.5 cm per sample, indicate the seasonality of the components, and the corresponding yearly ice thicknesses are listed in Table 6 (see the text for details).

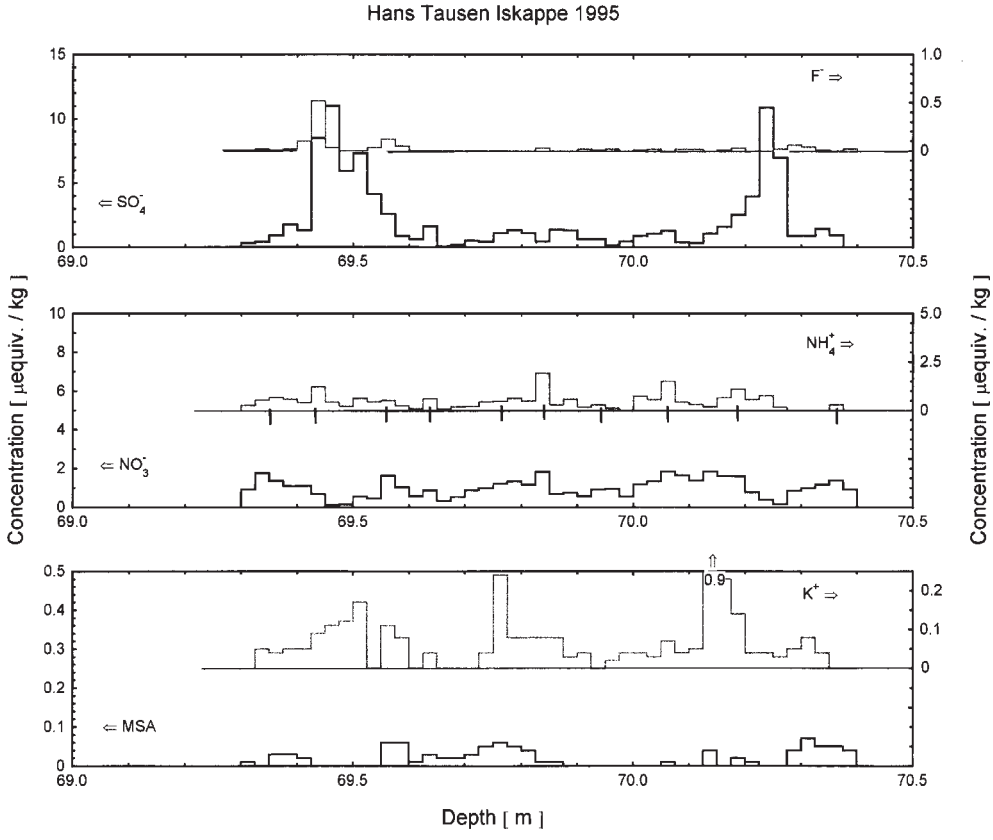

Figs. 15, 17, 19 and 21 show the concentration of F^{-} and SO_4^{2-},NH_4^{+} and NO_3^{-}, K^{+} and MSA at the same depth intervals as those in Figs. (14, 16, 18 and 20). The seasonality is demonstrated by the vertical marking on the NH_4^{+} and NO_3^{-} curves, and the results are listed in Table 6 (see the text for details).

Fig. 15.

Fig. 16.

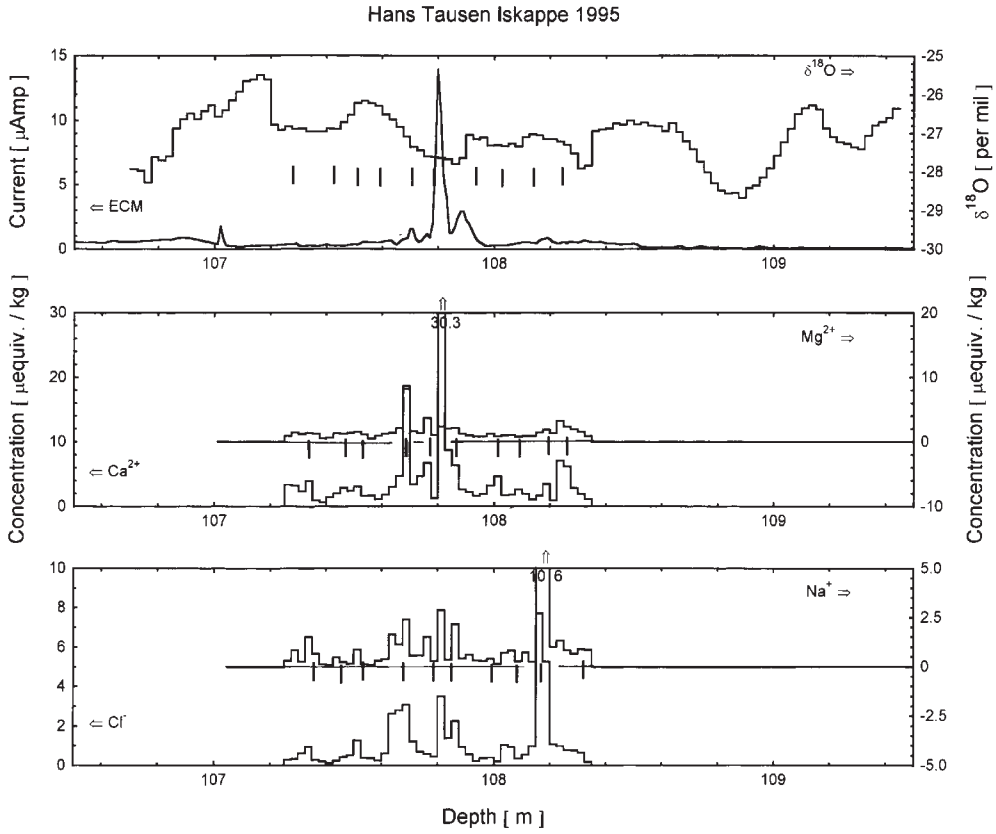
Hans Tausen Iskappe 1995
Current [μAmp]
⇐ ECM
δ18O ⇒
δ18O [per mil]
Concentration [μequiv. / kg]
⇐ Ca2+
30.3
Mg2+ ⇒
⇐ Cl-
10.6
Na+ ⇒
Depth [m]

Fig. 17.

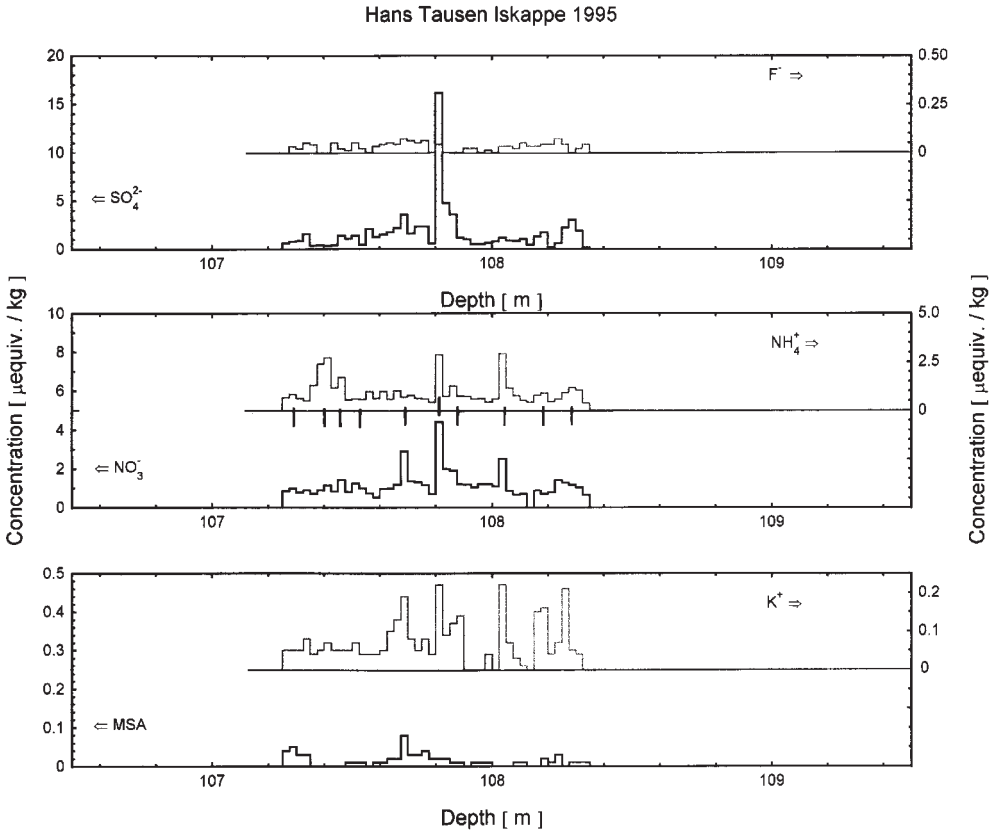
Hans Tausen Iskappe 1995
⇐ SO4 2-
F- ⇒
Depth [m]
Concentration [μequiv. / kg]
⇐ NO3-
NH4+ ⇒
⇐ MSA
K+ ⇒

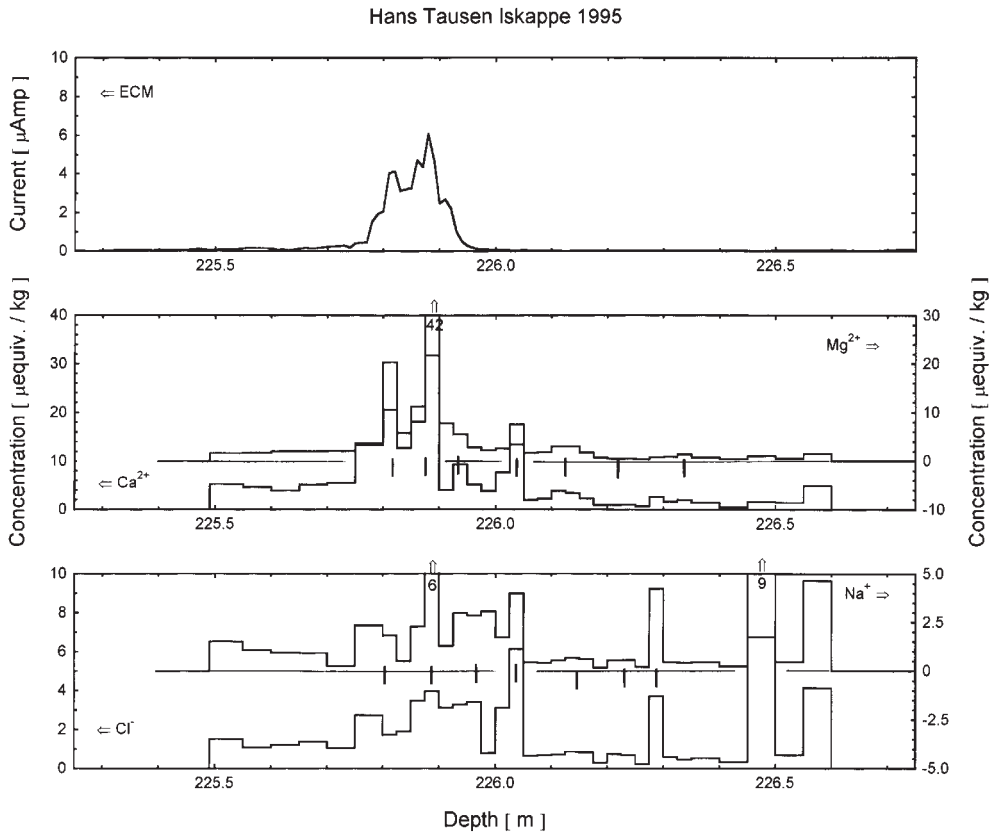
Hans Tausen Iskappe 1995
Current [μAmp]
⇐ ECM
Concentration [μequiv. / kg]
42
Mg2+ ⇒
⇐ Ca2+
6
9
Na+ ⇒
⇐ Cl-
Depth [m]

Fig. 18.

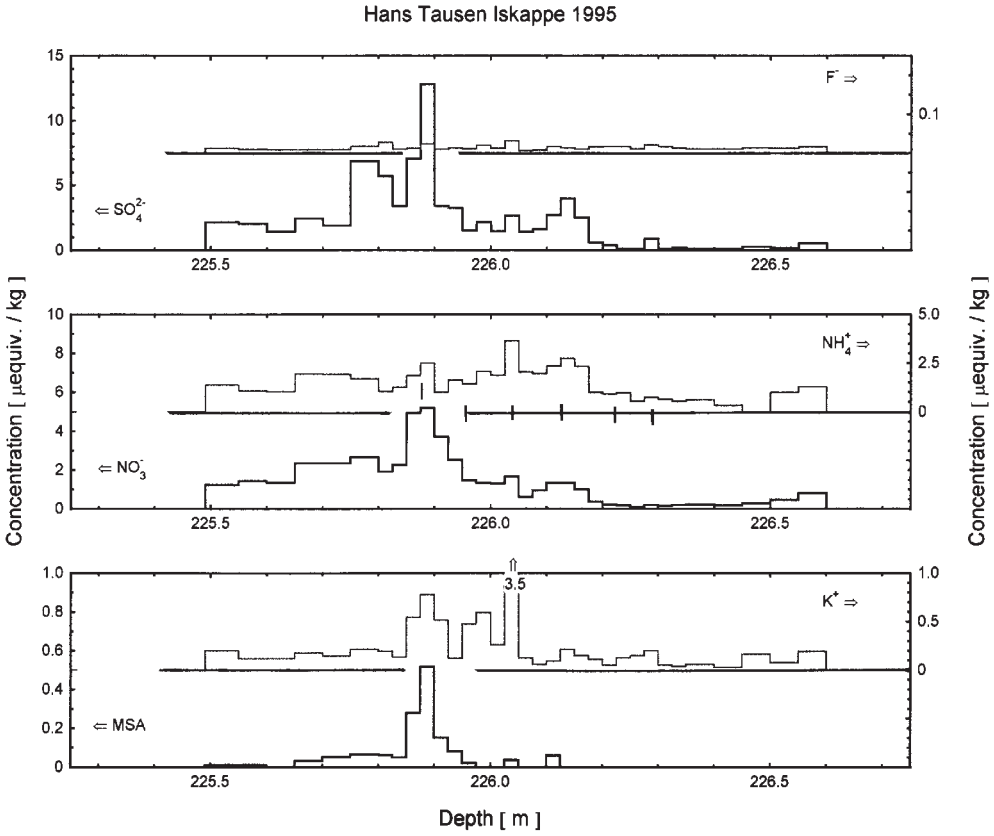
Hans Tausen Iskappe 1995
F- ⇒
⇐ SO4 2-
Concentration [μequiv. / kg]
NH4+ ⇒
⇐ NO3-
3.5
K+ ⇒
⇐ MSA
Depth [m]

Fig. 19.

Fig. 20.

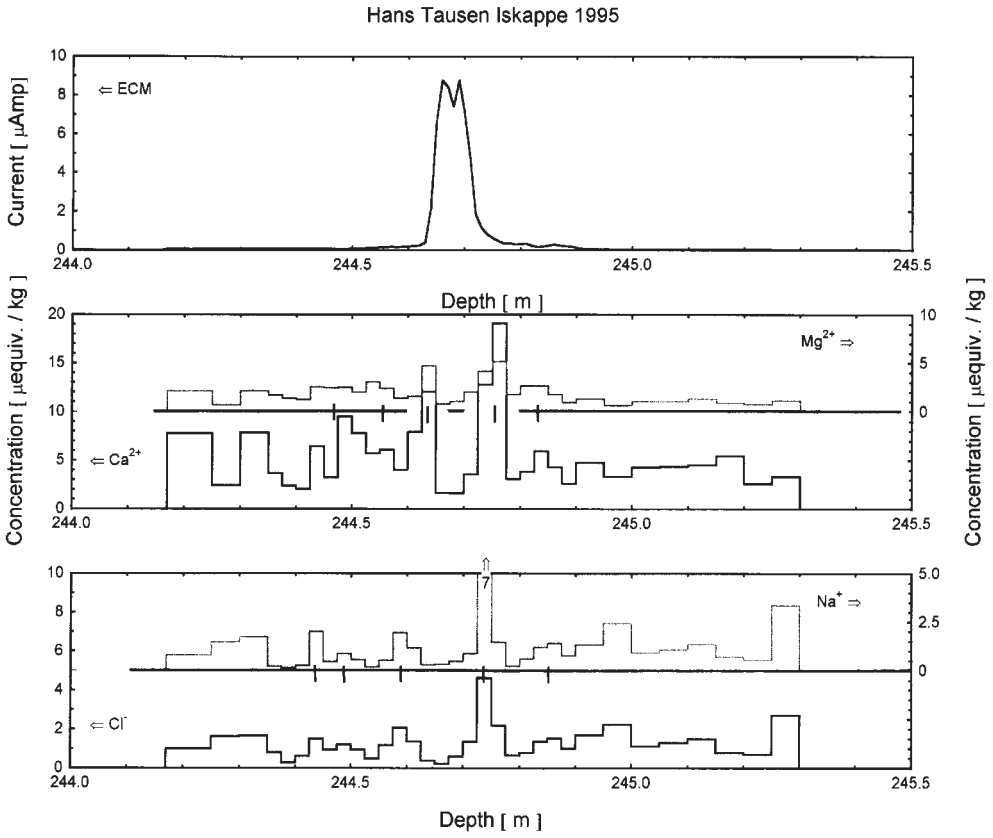
Hans Tausen Iskappe 1995
⇐ ECM
Current [µAmp]
Depth [m]
Concentration [µequiv. / kg]
Mg2+ ⇒
⇐ Ca2+
Na+ ⇒
⇐ Cl-
Depth [m]

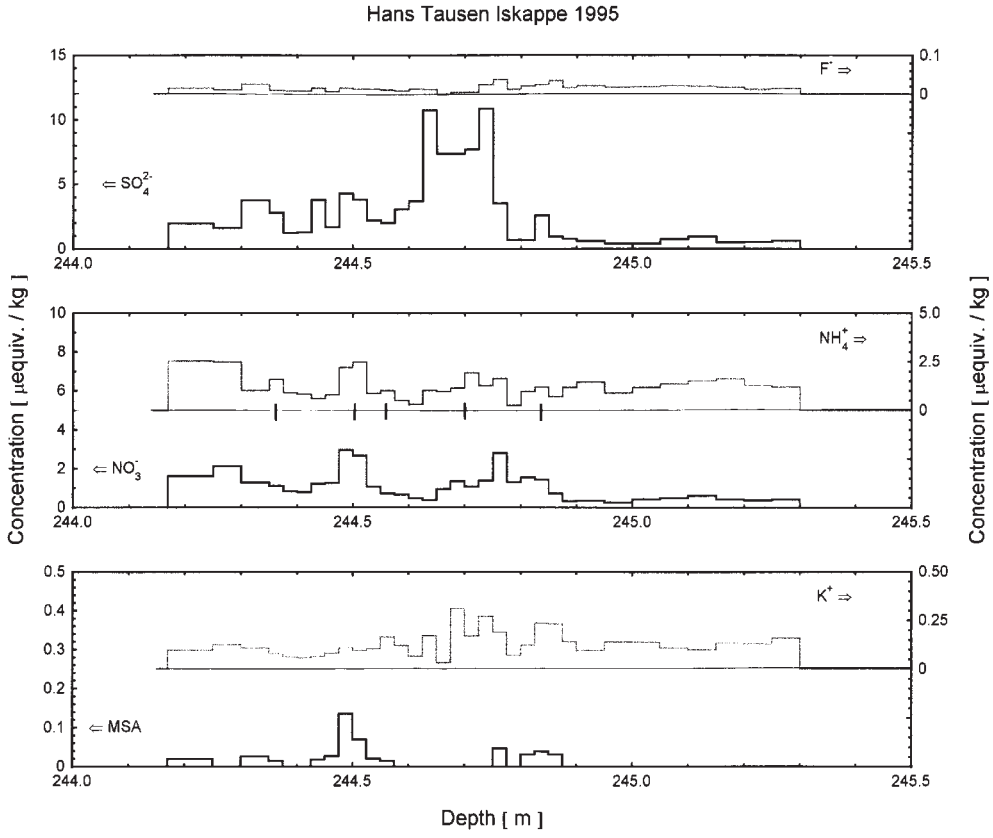
Hans Tausen Iskappe 1995
F- ⇒
⇐ SO4 2-
NH4+ ⇒
⇐ NO3-
K+ ⇒
⇐ MSA
Concentration [µequiv. / kg]
Depth [m]

Fig. 21.

haviour is not clearly demonstrated in the pit samples partly due to the high content of the dust which at HT amounts an order of magnitude higher than at GRIP, in average some 50,000 particles per ml at HT against some 5,000 per ml at GRIP (Steffensen *et al*. 1996). Also the frequent surface melting and the refreezing of the meltwater in the cold winter snow below can blur the stratigraphy by redistribution of water soluble ions. NO_3^- concentration shows distinct seasonal variation in polar ice (Risbo *et al*. 1981) with maximum in late summer precipitation (in the $\delta^{18}O$ maximum). In snow representing the last 50 years the seasonality pattern of NO_3^- has changed due to an anthropogenic input which partly has doubled the concentration (Mayewski *et al*. 1986), and partly changed the season signal into a double peak with an additional peak showing up in the early spring precipitation (at the Ca^{2+} and dust peaks) (Finkel *et al*. 1986). In Greenland ice the SO_4^{2-} signal does not show an unambiguous seasonal signal as found in Antarctica ice. This is mainly due to the difference in the relative strength of the active SO_4^{2-} sources. But what is observed in Greenland is a similar pattern as found in the NO_3^- with a pronounced early spring peak due to an anthropogenic input starting some 100 years ago and with a four time concentration increase in present precipitation.

In order to further investigate the seasonality of the chemical components in ice older than 100 years, we use the chemical data from the 4 depth intervals listed in Table 6 and based on a resolution of 2.5 cm per sample. This is the case for 88 samples of Figs. 14 – 21 where the 10 chemical components and the ECM current are arranged in the same way in all the figures, except for Fig. 16, where a detailed $\delta^{18}O$ profile is shown on the ECM current figure.

Mg^{2+} and Ca^{2+} show maximum in the spring, like dust (Figs. 14, 16, 18, 20).

Na^+ and Cl^- show maximum in the winter (Figs. 14, 16, 18, 20).

NH_4^+ and NO_3^- show maximum in the summer like $\delta^{18}O$ (Figs. 15, 17, 19, 21).

The vertical lines on the figures indicate the seasonality and the amounts of years in the records. Table 6 compiles these data and compare the consequent annual ice thicknesses with those determined by the acid volcanic layers from Table 3. The values based on the chemical series are not inconsistent with those based on ECM. It is interesting that the seasonality of the above 6 components show up considering that the annual resolution is based on only some 4 samples per year. This relative low resolution combined with the frequent melting, which causes redistribution of the water soluble ions, does not allow any conclusion on how the peaks show up within a year:

Na^+ and Cl^- before Mg^{2+} and Ca^{2+} before NH_4^+ and NO_3^-.

K^+ follows Mg^{2+} and Ca^{2+} and peaks at the same time. This is not marked by vertical lines on Figs. 15, 17, 19, 21 as it does not provide an independent yearly resolution because the main source of K^+ is terrestrial like for Mg^{2+} and Ca^{2+} in the HT ice.

F^- with volcanism as the dominant source does not show any seasonality (Figs. 15, 17, 19, 21).

SO_4^{2-} does not exhibit seasonal variations as distinct as e.g. NO_3^- (Figs. 15, 17, 19, 21). This is due to the varying strength of the various sources of SO_4^{2-}, with volcanism in a predominant role partly by major volcanism which creates high SO_4^{2-} peaks, and partly by non explosive emission of sulphurous gases which contribute to the sulfate background. Other sources to SO_4^{2-} in Greenland are terrestrial and marine biological processes. An important marine biological source is Dimethylsulfide [DMS, $(CH_3)_2S$] which is emitted from the ocean to the atmosphere where it is oxidized partly to methanesulfonic acid [MSA,

Table 7. Compares the amount of the deposited acid (as sulphuric acid) at HT and GRIP from 4 volcanic eruptions (VAD), and the corresponding magnitudes of the eruptions.

Event	Hans Tausen Iskappe		GRIP	
	VAD	Magnitude	VAD	Magnitude
	kg H_2SO_4/km^2	Mton H_2SO_4	kg H_2SO_4/km^2	Mton H_2SO_4
AD 1512	39	79	53	77
AD 1179	32	66	45	65
49 BC	38	77	140	194
244 BC	39	79	40	51

CH_3SO_3] and partly to SO_2. The branching ratio of this process is not well known (Saltzman 1995). Because the MSA concentrations at HT and at central Greenland sites like Crete and GRIP are low (~0.03 µequiv./kg) and at the same level (Osada and Langway 1993), (Legrand *et al.* 1997), the biological marine sources of MSA are remote and their contribution to the sulfate background is of less importance. This is quite different from Antarctica, where the marine biological processes are the dominant SO_4^{2-} source (Mulvaney and Peel 1988).

The data sets of Table 6 are also used in the discussion of the chemical composition of the volcanic signals and for the comparison to the corresponding volcanic signals in the GRIP ice core. The study comprises the volcanic events of:

AD 1512, Figs. 14-15; AD 1179, Figs. 16-17; 49 BC, Figs. 18-19 and 244 BC, Figs. 20-21.

The amount of deposited sulphuric acid per km^2 from volcanic eruptions depends upon the site of eruption and the magnitude of the eruption. To estimate the magnitude we compare the amount of volcanic acid deposited per km^2 (VAD) to the deposited amount of total β-activity from known atmospheric nuclear bomb tests (Clausen and Hammer 1988). VAD is calculated by integrating the amount of acid above the background value during the period of elevated acidity. VAD and the magnitude expressed in Mton H_2SO_4 are listed in Table 7 where we for comparison have assumed a high northern latitude (HNL) eruption site for the four events. The factor that converts HT VAD values into magnitude for a HNL eruption is $2.04 \cdot 10^9$ (see total β-activity section). The comparison to the magnitudes determined for GRIP (Clausen *et al.* 1997) shows agreement except for the 49 BC event where a factor of 2 occurs, however deviation of this size has been observed in other cases (Langway *et al.* 1988).

Generally for the chemistry of the four events we find sulfate as the dominant component and in the case of the AD 1512 and AD 1179 events we find significant amounts of F^- as found in the GRIP ice cores. The F^- records show the F^- distributed in the well recognised symmetrical pattern on the flanks of the sulfate peaks due to the post depositional replacement of F^-. Both events are assigned to high northern latitude eruption sites: The AD 1512 event is only seen in Greenland ice core records from the GRIP region and north of this location like the AD 1912 eruption of Katmai in Alaska. The AD 1179 event is, like all major Icelandic eruptions, found in all Greenland records covering this time period, and the event is assigned to the Katla eruption of AD 1179. The 49 BC event is like in other Greenland records a "pure" sulfate signal. The chemical composition of the 244 BC event differs from that found in the GRIP record. The GRIP signal consist of a substantial amount of Cl^- and F^- besides the sulfate. The lack of the Cl^- and F^- is probably

	Pit		AD 1512		AD 1179		49 BC		244 BC	
	HT	GRIP	HT	GRIP	HT	GRIP	HT	GRIP	HT	GRIP
Component	Concentration [µequiv./kg]									
F-	0.007	0.007	0.028	0.031	0.028	0.048	0.014	0.022	0.015	(0.109)
MSA	0.019	0.016	0.019	0.034	0.014	0.029	0.044	0.033	0.015	0.023
Cl^-	1.48	0.95	0.88	0.34	1.21	0.37	1.90	0.39	1.29	(4.47)
NO_3^-	1.40	2.12	1.00	1.20	1.17	1.29	1.41	1.41	1.07	1.03
SO_4^{2-}	2.50	2.62	2.09	1.26	1.67	1.38	2.31	1.37	2.90	2.90
Na^+	1.30	0.45	0.66	0.18	1.04	0.26	1.75	0.33	1.15	0.47
NH_4^+	1.15	0.40	0.45	0.46	0.93	0.58	1.43	1.02	1.24	0.28
K^+	0.58	0.08	0.08	0.02	0.07	0.05	0.31	0.09	0.13	0.05
Mg^{2+}	1.43	0.19	1.07	0.17	1.55	0.14	3.35	0.22	1.91	0.11
Ca^{2+}	2.95	0.39	1.94	0.40	3.88	0.37	6.55	0.49	5.46	0.37

Table 8. Compares the concentration values of 10 chemical compounds from common time intervals in the HANS TAUSEN and GRIP ice cores. For the parentheses at the 244 BC GRIP values, see text.

due to the strong hydrophilic character of these components, also the 244 BC signal is the last acid peak of the ECM record where the ice core at this depth consists of some 75% refrozen meltwater.

Other volcanic signals like Laki AD 1783 and Eldja AD 934 found in the HT95 Ice core are discussed by Stampe (Stampe 1997).The HT chemical data sets presented in Figs. 13-21 are compared to GRIP data which represent the same time intervals as the HT data, and the data are presented in Table 8. The HT data deviate from those presented in Table 5, especially the SO_4^{2-} values due to the presence of major volcanic signals in the data sets.

The $\delta^{18}O$ record

Detailed $\delta^{18}O$ records with annual resolutions exist from HT75, HT76, HT94 and HT95 and are shown on Figs. 22-25 provided with time markers from recognizable events. The sample frequency of the 4 records corresponds to 50, 50, 20 and 40 samples per m, respectively. Other $\delta^{18}O$ records presented here are the records of HT75, HT76, SC95 and MC95 which is only given to the same age level as covered in SC75 and SC76. The 4 latter $\delta^{18}O$ records are presented in Figs. 3 and 26 in resolutions from 2 to 6 samples per m. Table 1 shows the mean annual accumulation rates and the $\delta^{18}O$ means of common time intervals represented in the ice cores. Generally the data show increasing $\delta^{18}O$ and accumulation values from AD 1783 to 1975, and the opposite trend during the period 1975 to 1995. The $\delta^{18}O$ mean value of –26.2 per mil and the mean annual temperature of –21°C for HT95, places Hans Tausen Iskappe on the Greenland far North and North East line of the $\delta^{18}O$ – temperature curve, which includes locations like Spitsbergen and Station Nord, and indicates that the air masses take up some water vapour from the Arctic oceans (Dansgaard *et al.* 1973). The entire $\delta^{18}O$ record of MC95 is discussed by Hammer *et al.* (2001).

The total β-activity record

In the 1950'ies and the early 1960'ies mainly the Americans and the Russians performed thermonuclear bomb tests in the atmosphere. Radioactive debris from these tests was deposited on the polar ice caps by precipitation, and the polar ice became stratified by the radioactive isotopes from the debris. Today mainly the radioactive isotopes ^{90}Sr and ^{137}Cs remain, and these isotopes were identi-

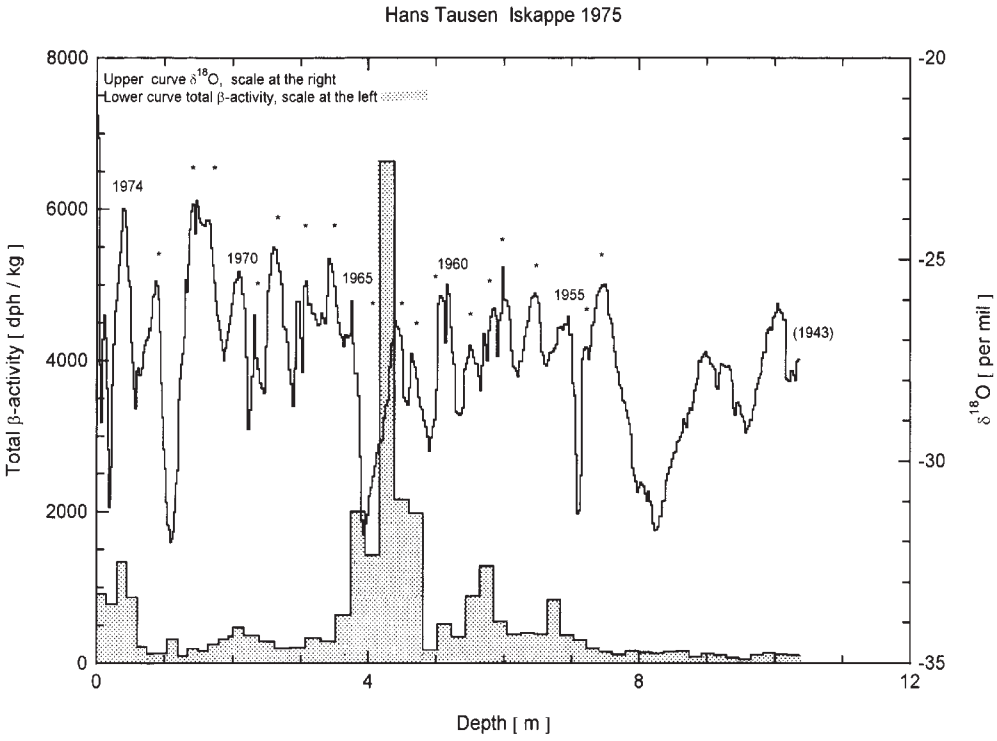

Fig. 22. A detailed $\delta^{18}O$ record (in 2.5 cm resolution) of the top 10 m of the HT75 ice core (scale to the right), and a total β-activity record (scale to the left), provide the ice core with a calendar year dating back to 1953, and suggest 1943 at the bottom depth 10.4 m of the detailed sampling.

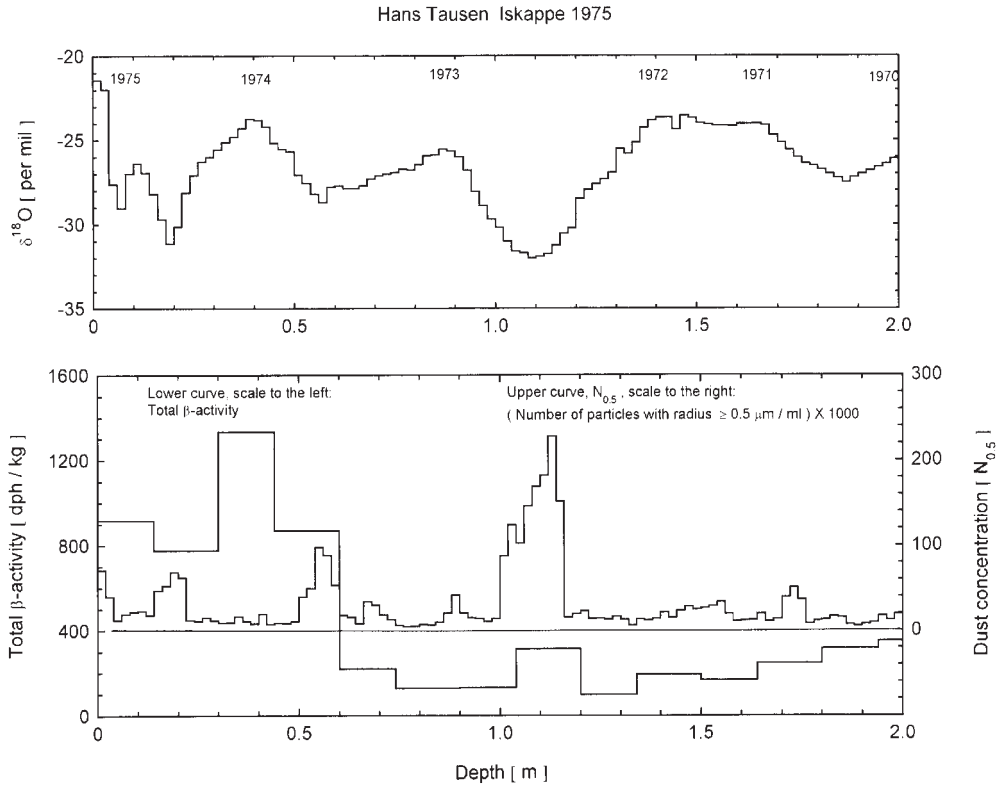

Fig. 23. The figure shows a blown up version of the top 2 m presented in Fig.22 ($\delta^{18}O$ and total β-activity) and a high resolution dust concentration profile (scale to the right) which supports the calendar year dating placed on the $\delta^{18}O$ curve, by the clear early spring peaks of 1971 to 1975.

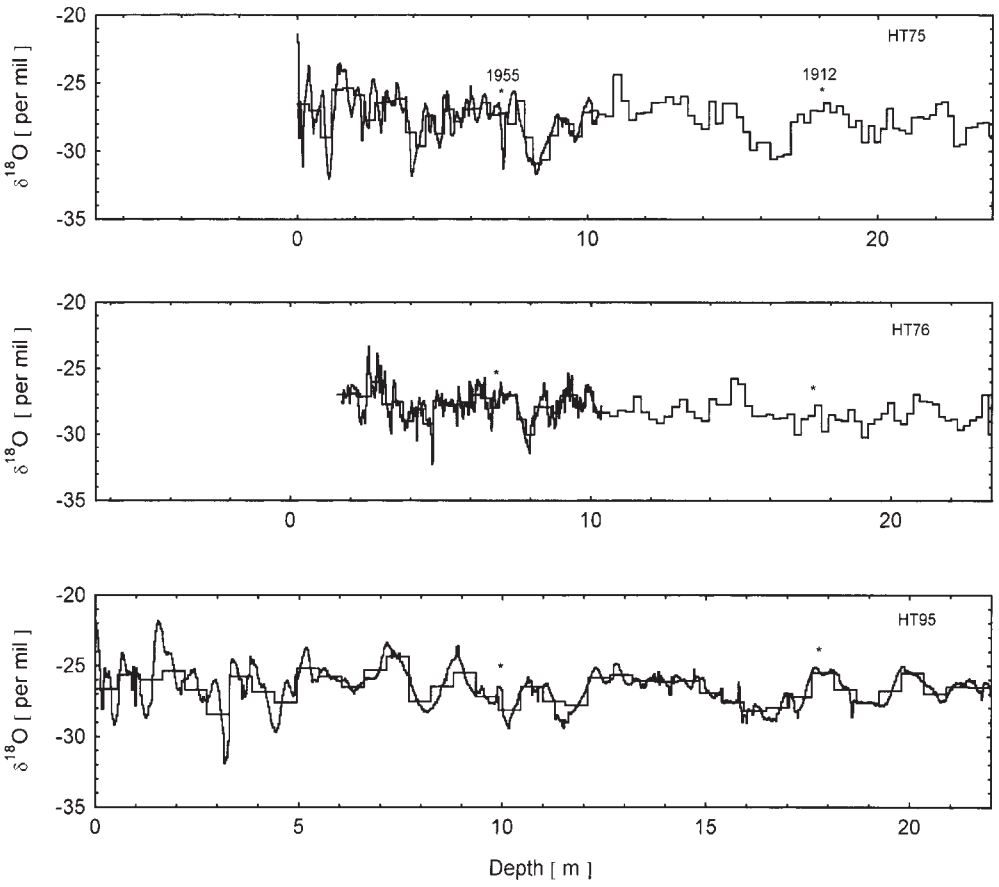

Fig. 24 shows the $\delta^{18}O$ of HT75, HT76 and HT95 (Fig. 25 contains in details the top 6 m of the HT95 record). The 22 m long record of the HT95 represents the length of the detailed (2.5 cm) $\delta^{18}O$ sampling, and the HT75 and HT76 records are locked to the HT95 record at the fixed points of 1955 and 1912 (marked by asterisks at the HT76 and HT95 records). Besides the detailed $\delta^{18}O$ curves, also the $\delta^{18}O$ curves in a lesser resolution are shown. The resolution is 55 cm per sample in the case of HT95, and some 24 cm in the case of HT75 and HT76.

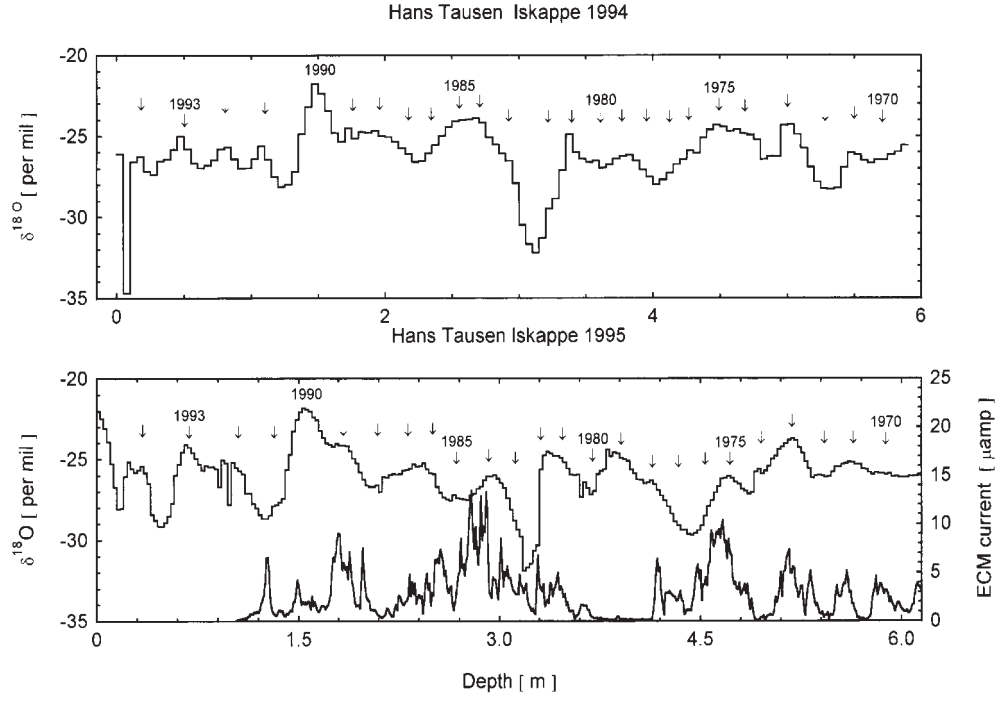

Fig. 25 presents the $\delta^{18}O$ curves of the HT94 (in a 5 cm resolution) and the top 6 m (in a 2.5 cm resolution) of the MC95 profile (see also Fig. 24) provided with the ECM current (lower right scale). The two depth scales are locked together at 1990 and 1975. The arrows suggest the summer positions of a calendar dating of the two records, and the ECM curve supports this dating.

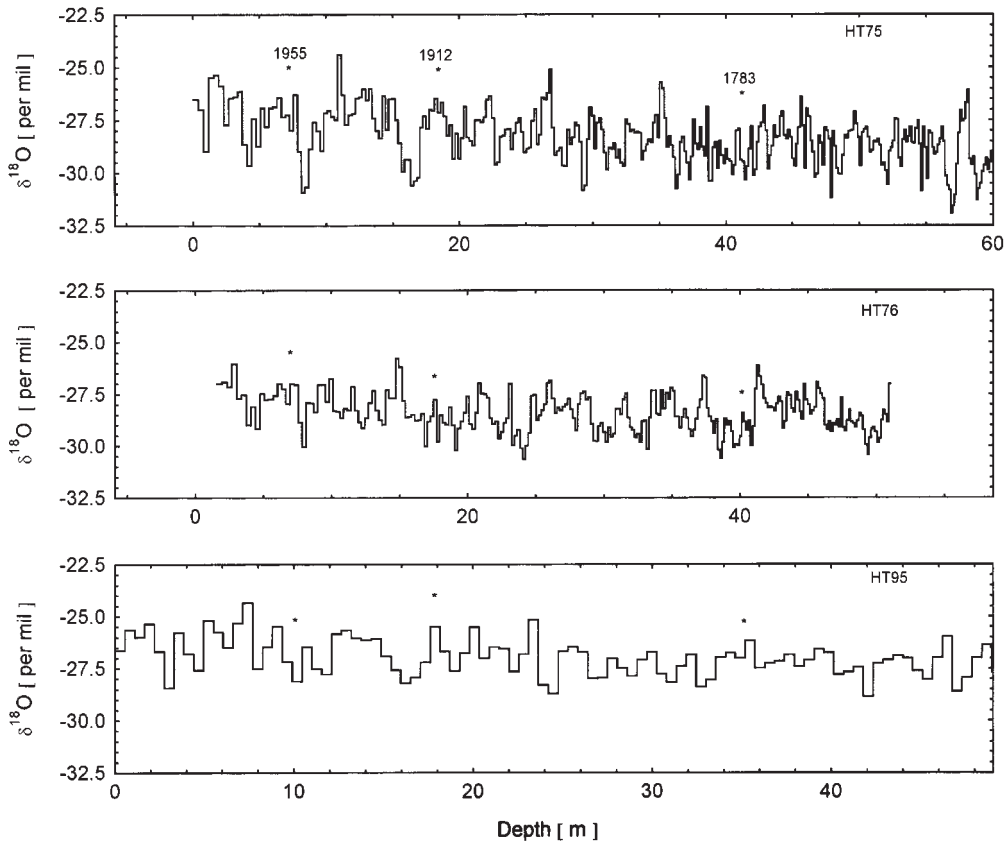

Fig. 26 shows the entire $\delta^{18}O$ records of the HT75 and HT76 ice cores in a resolution of some 15-16 cm of ice equivalent per sample. These curves are locked to the HT95 record at the fixed points of 1955, 1912 and 1783 shown by asterisks on the HT76 and HT95 records. The top some 20 m are shown in details in Fig. 24.

fied by measurement of the total β-activity of ice core samples.

Fig. 22 shows an example of a total β-activity record and a detailed $\delta^{18}O$ record from HT75, and exhibits the typical shape of the total β-acivity records known from other Greenland locations (Clausen and Hammer 1988). This shape includes the raise in 1954 to above the natural total β-activity background which mainly consists of ^{210}Pb (due to the American test series at low northern latitudes (LNL) in the early 1950'ies), a relative minimum (due to the declared moratorium on nuclear testing from November 1958 to September 1961) and the absolute maximum (mainly due to the Russian test series at high northern latitudes (HNL) in the early 1960'ies). Also the record shows a maximum and an increase around 1970 and 1974, respectively. These peaks are probably due to the Chinese test series at 40° N at Lop Nor and they are found in ice cores from other Greenland sites as well (Clausen and Hammer 1988). The total β-acivity records can be used to estimate the magnitude of major volcanic eruptions from known eruption sites. At Hans Tausen Iskappe we find a total β-acivity deposition of 11.1 mCi / km^2 originating from the amount of 22.6 MCi injected into the atmosphere by the Russian test series at HNL in 1962-66. This determines the factor of $2.04 \cdot 10^9$ used in the chapter of the chemical records. The corresponding factor for an eruption site at LNL is $5.89 \cdot 10^9$ based on a deposition of 1.63 mCi / km^2 from 9.6 MCi injected into the atmosphere by the American test series at LNL in 1953-55.

Dating of the ice core

The dating of the ice cores is based on the records of acidity (ECM), water soluble ion concentrations (e.g. nitrate and sodium), $\delta^{18}O$ and total β-activity. Table

	HT 1994 Snow pit			HT 1995 Snow Pit #1			HT 1995 Snow Pit #2			HT 1995 Main Core			Mean-annual rate of-accumulation
	Depth, start of year		Annual rate of	Depth, start of year		Annual rate of	Depth, start of year		Annual rate of	Depth, start of year		Annual rate of	
Year AD	m of snow	m of ice	accumu-lation	m of snow	m of ice	accumu-lation	m of snow	m of ice	accumu-lation	m of snow	m of ice	accumu-lation	m of ice/year
1995				0			(0.125	0.043	0.043)	(0.175	0.061	0.061)	
1994	(0.30	0.104	0.104)	0.400	0.140	0.140	0.550	0.194	0.151	0.475	0.167	0.106	0.132
1993	0.65	0.229	0.125	0.775	0.274	0.134	0.975	0.346	0.152	0.950	0.337	0.170	0.145
1992	0.95	0.337	0.108	1.075	0.382	0.108	(1.100	0.391	0.045)	1.250	0.444	0.107	0.108
1991	1.25	0.444	0.107	(1.100	0.391	0.009)				1.400	0.507	0.063	0.085

Table 9. Shows the annual rate of accumulation at 4 different locations around the HT95 drilling site. The dating in calendar years is based on the $\delta^{18}O$ records, dust measurements and chemical components like Ca^{2+}, Mg^{2+} and Na^{+}, Cl^{-} and NH_4^{+}, NO_3^{-} (see Fig. 13, which exhibits the data from snow Pit#1). The 1995 density record is used for all sites, and the resolution of the records is 5 cm for the HT94 record and 2,5 cm for the HT95 records. Parenthesis means an incomplete year in the record.

9 shows the annual rate of accumulation for the period 1991-95 determined by $\delta^{18}O$ measurements performed on snow pit samples from 4 different locations at the HT95 drilling site and the data from snow pit #1 are exhibited in Fig. 13. Fig. 27 shows the HT95 time scale as defined by the volcanic fixed points plotted versus a depth scale in m of ice equivalent. Fig. 6 shows ECM pins on a time scale from GRIP and Hans Tausen. The fixed points of the dating (marked by asterisks) are from the $\delta^{18}O$ records (see above): 1947, 1963 and 1983, and from major volcanic eruptions known from other Greenland ice core ECM records covering the last 200 years: e.g. AD 1912, 1816, 1810 and 1783. For ice cores representing precipitation over the last 1000 years especially the period AD 920 to AD 1275 is interesting, because in this time interval we find three large volcanic signals at AD 934, 1179 and 1259 and they are among the largest signal found during the last 11,500 year long Holocene period (Clausen *et al*. 1997). The three signals are found in all Greenland ice core records which reach the depth corresponding to these ages, and in average one signal of this type appears per century. The AD 1259 signal is, besides being a fixed point for dating of artic ice cores (also found in Canadien ice cores (Fisher and Koerner 1988)) also identified in antarctic ice cores and thus serves as an interhemispheric fixed point (Langway *et al*. 1988). For the time period between 1000 and 2000 years ago we find acid signals corresponding to AD 527, 49 BC and 244 BC (Clausen *et al*. 1997), and as mentioned in the ECM section no ECM peak signals are seen below the depth of 250 m.

Conclusion

Information from the ECM measurements and the chemical analyses are available despite the large impurity content from local sources and the relatively high temperatures during part of the ECM measurements. Major volcanic eruptions can be identified and used as time markers. Seasonal variations are preserved in the $\delta^{18}O$ records from the top layers, and chemical compounds like e.g. NO_3^{-}, Ca^{2+} and dust measured on discrete core sequences, show seasonality. The average annual ice thickness (λ) is some 10 cm of ice equivalent per year down to the depth of 244 m, and a detailed dust profile covering some 5 m close to bottom indicates almost an unchanged λ at this depth (Hammer *et al*. 2001). This suggests an age of some 3000 years for the bottom near layers. The observation that no significant thinning of annual layers is

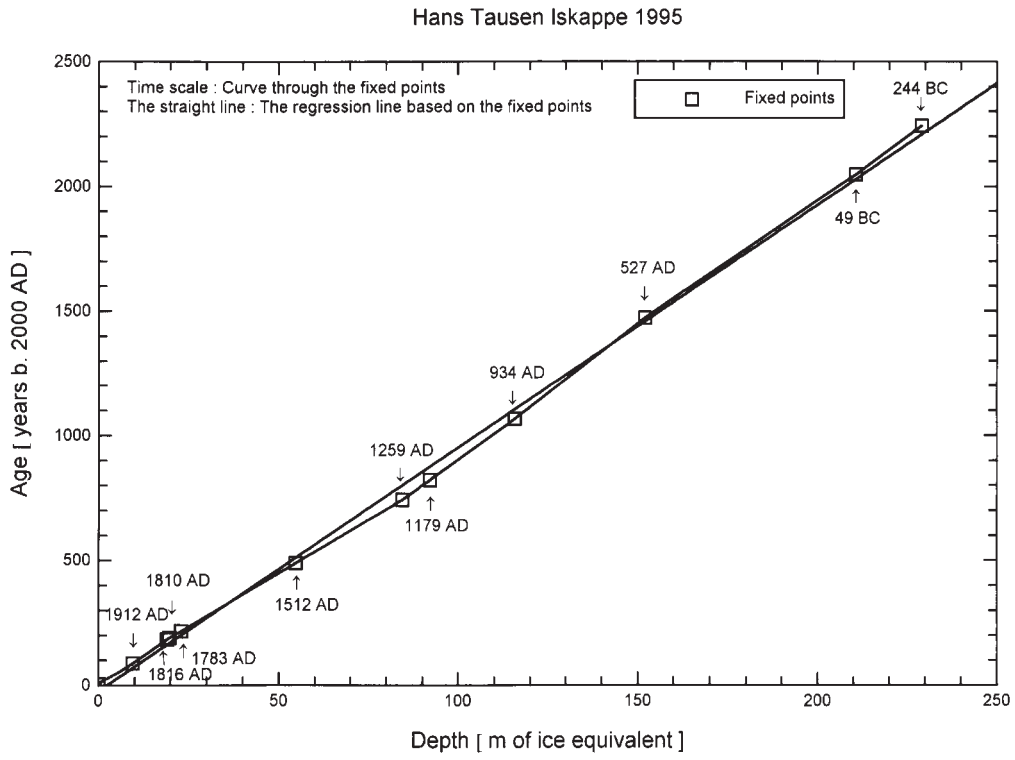

Fig. 27 presents a time scale (the line segments though the origin and the squares) for the HT95 ice core based on 11 prominent volcanic eruptions also listed in Tables (3 and 4). The regression line based on the fixed points: y = 9.74x –23.1 corresponds to an average annual ice thickness of 10.3 cm of ice equivalent per year for the time period represented by this depth interval.

observed, supports other findings (Keller *et al.* 2001) that the Hans Tausen Iskappe is not in mass balance.

Acknowledgments

We want to thank the *Danish Natural Science Research Council* (SNF), *the Climate Change Research Program* under the *Nordic Environmental Research Program* (the *Nordic Council of Ministers*) and the EU DGXII project *MilEClim* for financial support. Also we want to thank the personnel at Station Nord for hospitality and logistic support.

References

Blaker, M. R. and J. S. Peel 1997. Lower Cambrian trilobites from North Greenland. Meddelelser om Grønland Geoscience 35: 1-145.

Clausen, H. B. and C. U. Hammer 1988. The Laki and Tambora eruptions as revealed in Greenland ice cores from 11 locations. *Annals of Glaciology* 10: 16-22.

Clausen, H. B. *et al.* 1995. 1250 years of global volcanism as revealed by Central Greenland Ice Cores. In: *Ice Core Studies of Global Biogeochemical Cycles*. R. J. Delmas. New York, Springer-Verlag. 30: 175-194.

Clausen, H. B. *et al.* 1997. A comparison of the volcanic records over the past 4000 years from the Greenland Ice Core Project and Dye3 Greenland ice cores. *Journal of Geophysical Research* 102(C12): 26707-26723.

Clausen, H. B. and C. C. Langway, Jr. 1989. The ionic deposits in polar ice cores. In: *Dahlem Konference: The Environmental Record in Glaciers and Ice Sheets*. H. Oeschger and C. C. Langway, Jr. New York, John Wiley: 225-248.

Dansgaard, W. *et al.* 1973. *Stable Isotope Glaciology.* Meddelelser om Grønland 197(2): 5-53.

Finkel, R. C. *et al.* 1986. Changes in precipitation chemistry at Dye 3, Greenland. *Journal of Geophysical Research* 91(D9): 9849-9855.

Fisher, D. A. and R. M. Koerner 1988. The effects of wind on $\delta^{18}O$ and accumulation give an inferred record of seasonal $\delta^{18}O$ amplitude from the Agassiz ice cap, Ellesmere Island, Canada. *Annals of Glaciology* 10: 34-37.

Hammer, C. U. 1977. Dating of Greenland ice cores by micro-particle concentration analyses. In: *Proc. of Symp. on Isotopes and Impurities in Snow and Ice, I.U.G.G. XVI, General Assembly, Grenoble Aug. Sept., 1975*. Washington D.C.: 297-301.

Hammer, C. U. 1980. Acidity of polar ice cores in relation to absolute dating, past volcanism, and radio-echoes. *Journal of Glaciology* 25: 359-372.

Hammer, C.U, S. J. Johnsen, H. B. Clausen, D. Dahl-Jensen, N. Gundestrup and J. P. Steffensen 2001. The paleo-climatic record from a 345 m long ice core from the Hans Tausen Iskappe. Meddelelser om Grønland Geoscience, this volume pp. 87-95.

Keller, K., C. S. Hvidberg, N. Gundestrup and P. Jonsson 2001. Surface Movement and Mass Balance at the Hans Tausen Drill Site determined by use of GPS. Meddelelser om Grønland Geoscience, this volume pp. 115-122.

Langway, C. C., Jr. *et al.* 1988. An inter-hemispheric volcanic time-marker in ice cores from Greenland and Antarctica. *Annals of Glaciology* 10: 102-108.

Legrand, M, *et al.* 1997. Sulfur-containing species (methanesulfonate and SO_4) over the last climatic cycle in the Greenland Ice Core Project (central Greenland) ice core. *Journal of Geophysical Research* 102(C12): 26663-26679.

Madsen, K. N. and T. Thorsteinsson 2001. Texture, fabrics, and melt layer stratigraphy in the Hans Tausen Ice Core, North Greenland – indications of late Holocene ice cap generation? Meddelelser om Grønland, Geoscience, this volume pp. 97-114.

Mayewski, P. A. *et al.* 1986. Sulfate and Nitrate Concentrations from a South Greenland Ice Core. *Science* 232: 975-977.

Mulvaney, R. and D. A. Peel 1988. Anions and cations in ice cores from Dolleman Island and the Palmer Land plateau, Antarctic Peninsula. *Annals of Glaciology* 10: 121-125.

Osada, K. and C. C. Langway 1993. Background levels of formate and other ions in ice cores from inland Greenland. *Geophysical Research Letters* 20 (23): 2547-2650.

Risbo, T. *et al.* 1981. Supernovae and nitrate in the Greenland Ice Sheet. *Nature* 294: 637-639.

Saltzman, E. S. 1995. Ocean/Atmosphere Cycling of Dimethylsulfide. In*: Ice Core Studies of Global Biogeochemical Cycles.* R. J. Delmas. New York, Springer-Verlag. 30: 65-89.

Simkin, T. and L. Siebert 1994. *Volcanoes of the World.* Tucson, Ariz., Geoscience Press.

Stampe, M. 1997. *Vulkanske vidnesbyrd i iskerne fra Hans Tausen*. Master of Science thesis, University of Copenhagen, Geophysical Department, Niels Bohr Institute, 93 pp.

Steffensen, J. P. *et al.* 1996. On the spatial variability of impurity content and stable isotope composition in recent Summit snow. In: *Chemical Exchange Between the Atmosphere and Polar Snow.* E. W. Wolff and R. C. Bales. New York, Springer-Verlag. 43: 607-616.

Steffensen, J. P. *et al.* 2001. Microparticles, soil derived chemical components and sea salt in the Hans Tausen Iskappe ice core from Peary Land, North Greenland." Meddelelser om Grønland Geoscience, this volume pp. 151-160.

Sverdrup, H. U. *et al.* 1942. *The Oceans.* New York, Prentice Hall Inc.

Wedepohl, K. H., Ed. 1969. *Handbook of Geochemistry.* New York, Springer-Verlag.

Wolff, E. W. 1995. Nitrate in polar ice. In: *Global Biochemical Cycles in Polar Ice*. R. J. Delmas. New York, Springer-Verlag. 30: 195-224.